Journal Pre-proof

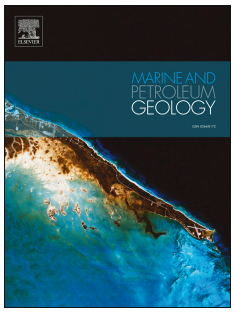

The transition from normal marine to evaporitic conditions recorded in a cold seep environment: The Messinian succession of Northern Italy

S. Conti, C. Argentino, M. Bojanowski, C. Fioroni, S. Giunti, B. Kremer, D. Fontana

PII: S0264-8172(23)00523-8

DOI: https://doi.org/10.1016/j.marpetgeo.2023.106617

Reference: JMPG 106617

To appear in: *Marine and Petroleum Geology*

Received Date: 2 August 2023

Revised Date: 6 November 2023

Accepted Date: 21 November 2023

Please cite this article as: Conti, S., Argentino, C., Bojanowski, M., Fioroni, C., Giunti, S., Kremer, B., Fontana, D., The transition from normal marine to evaporitic conditions recorded in a cold seep environment: The Messinian succession of Northern Italy, *Marine and Petroleum Geology* (2023), doi: https://doi.org/10.1016/j.marpetgeo.2023.106617.

The transition from normal marine to evaporitic conditions recorded in a cold seep environment: the Messinian succession of Northern Italy

Conti S.[1], Argentino C.[2], Bojanowski M.[3] Fioroni C.[1], Giunti S.[3], Kremer B.[4], Fontana D.[1*]

[1]Dept of Chemical and Geological Sciences, University of Modena and Reggio Emilia, Modena, Italy

[2] Department of Geosciences, UiT The Arctic University of Norway, Tromsø, Norway

[3] Institute of Geological Sciences, Polish Academy of Sciences, Warszawa, Poland

4 Institute of Paleobiology, Polish Academy of Sciences, Warszawa, Poland

*Corresponding author

Keywords: seep-carbonate, microbialites, Messinian, methane oxidation, northern Apennines

Abstract

Messinian pre-evaporitic seep carbonates outcropping in the Tuscan-Romagna area share a common upward stratigraphic trend: massive seep carbonates rich in large lucinids, modiolids and planktonic foraminifera pass upward to horizontally laminated carbonates free of macrofauna and foraminifera. A transitional macrofauna-free facies marks the passage in some sections, sometimes with faint lamination. Thin section petrography, SEM-EDS analyses, and X-ray diffraction revealed a high textural and mineralogical variability between the studied sections and facies. In general, the upward facies transition is associated with a switch from massive

packstone/grainstone with complex carbonate mineralogy to laminated mudstone microfacies with monomineralic, mostly dolomitic, carbonate composition. The $\delta^{13}C$ values of all facies indicate domination of methane-derived carbon, thus demonstrating a methane-charged sedimentary setting with precipitation of authigenic carbonates induced by anaerobic oxidation of methane. The transitional and laminated facies contain several structures typical of microbial sediments, such as peloids, filamentous features, clotted micrite, fibrous cement, and frequent fenestrae; web-like structures are remnants of cyanobacterial mats and resemble Entophysalidaceae thriving at the bottom of the Messinian sea. The distinctive depositional and biotic switch (abrupt disappearance of macrofauna and planktonic foraminifera, predominance of dolomite over calcite, absence of aragonite, presence of horizontal lamination) reflects important environmental changes taking place in the basin. The rise of $\delta^{18}O$ from the massive, through transitional, to the laminated facies suggests either a drop of bottom-water temperature or an increase of salinity. Nevertheless, other paleoenvironmental changes must have co-occurred in order to account for the dramatic facies shift observed. We hypothesize that this change could reflect the development of water-column stratification with respect to both salinity and oxygen concentration shortly before the Messinian Salinity Crisis.

1 Introduction

Cold seeps are marine environments marked by the subsurface migration of methane and other alkanes from underlying hydrocarbon and gas hydrate reservoirs toward the seafloor (Judd and Hovland, 2007; Suess, 2014). Life at cold seeps is mainly linked to the consumption of reduced compounds, i.e. methane (CH_4) or hydrogen sulfide (H_2S), by chemosynthetic microbial communities forming biofilms or living in symbiotic relationship with higher organisms, tubeworms, clams, mussels (Sahling et al., 2002; Dreier and Hoppert, 2014; Levin et al., 2016). The type of habitat observed at the seafloor is controlled by geochemical fluxes through the sediment and redox conditions in bottom waters (Fischer et al., 2012; Argentino et al., 2022).

Microbial mats tend to dominate areas of intense methane seepage due to their high tolerance to dissolved sulfide (Schulz et al., 1999; Jørgensen et al., 2010) and their capacity to survive periodic bottom water anoxia by using internally accumulated nitrate (Kalanetra et al., 2005). These microbial mats are dominated by sulfide-oxidizing bacteria like *Thioploca*, a large filamentous sulfide-oxidizing bacteria that has the capability to store nitrate (Fossing et al., 1995; Grünke et al., 2012). The habitats surrounding the microbial mats are inhabited by chemosymbiotic organisms requiring exposure to well-oxygenated conditions for their metabolic processes (Dubilier et al., 2008). Below the seafloor, methanotrophic archaea and sulfate-reducing bacteria work in syntrophic partnership to perform sulfate-driven anaerobic oxidation of methane (AOM) (Boetius et al., 2000; Cochran et al., 2022). AOM maintains H_2S fluxes to surface communities and generates alkalinity eventually leading to the precipitation of methane-derived authigenic carbonates (MDACs). These carbonates represent excellent archives of the history of seepage (Crémière et al., 2016; Bojanowski et al., 2021; Himmler et al., 2022;), and provide information on the redox conditions that accompanied carbonate precipitation (Feng et al., 2009; Hu et al., 2014; Smrzka et al., 2016; Argentino et al., 2020). Carbonates can incorporate remains of chemosynthetic fauna (shells, biomarkers) and display peculiar sedimentological and petrographic features preserving the signatures of microbial activity, e.g. laminations and peloids (Himmler et al., 2022), and of fluid expulsion processes, i.e. breccias, conduits, fractures (Conti et al., 2008; 2014). MDACs carry a unique carbon isotope composition typically depleted in ^{13}C leading to $\delta^{13}C$ values < -30‰ marking the incorporation of methane-derived carbon (Judd et al., 2020).

Although the biogeochemistry of methane oxidation and MDAC formation at cold seeps have been widely investigated in normal salinity marine settings, these processes at hypersaline conditions remain largely unconstrained in the fossil record due to the paucity of data. AOM activity is limited at high salinity conditions by bioenergetic constraints and only a few studies detected this process at modern hypersaline seeps (Oren, 2011; Cao et al., 2015; Joye, 2020).

However, it has also been demonstrated that in spite of a low energy yield of AOM, microorganisms carrying this reaction can thrive in salinity up to halite saturation (Maignien et al., 2013), have been reported from fossil settings (Ziegenbalg et al., 2010, 2012), and may therefore be expected to occur in many hydrocarbon brine pools (Orcutt et al., 2010; Lazar et al., 2011; Joye, 2020). For investigation of the dynamics and long-term evolution of cold seeps and AOM in high salinity conditions, ancient MDAC onshore outcrop analogs can be particularly valuable, because the site accessibility allows for high-resolution sampling and unconstrained investigation of the exposed carbonate deposits (Agirrezabala et al., 2013; Argentino et al., 2019).

Extreme salinity conditions affected large areas of the Mediterranean basin during the Messinian Salinity Crisis (MSC) in the Late Miocene (between 6.0 and 5.3 Ma, Hsu et al., 1973; Rouchy and Caruso, 2006, Manzi et al., 2011; Garcia-Veigas et al., 2020), but spatial and temporal environmental variability in the basin remains unclear (Mastandrea et al., 2010). The origin of the Messinian laminated authigenic carbonates known in the literature as the "Calcare di Base" (CDB) occurring at the base of the Messinian evaporites is controversial, mainly due to the scarcity of fossils and well-defined sedimentary structures (Cosentino et al., 2013; Tzevahirtzian et al., 2022). It is not clear whether CDB formed in shallow or in deep waters and the genesis (evaporitic or microbial) is debated (Manzi et al., 2011). Some authors argued that these carbonates precipitated during evaporitic and hypersaline conditions as suggested by some positive $\delta^{18}O$ values and laminated-stromatolitic structures (Ziegenbalg et al., 2012; Birgel et al., 2014), originally interpreted as remains of benthic algae (Vai and Ricci Lucchi, 1977) and later as generated by cyanobacteria consistent with a relatively shallow water depositional environment (Natalicchio et al., 2013). According to Borrelli et al. (2021) during the CDB deposition, an arid climate regime alternated with intermittent humid phases and conditioned the establishment of microbial-mediated carbonate production along a sabkha-type environment with extensive hypersaline coastal lagoons. This interpretation is also supported by the recognition that carbonate lamination in CDB is associated with faecal pellets of brine shrimps (Natalicchio et al., 2013),

confirming shallow and hypersaline depositional conditions. Other authors (Oliveri et al., 2010; Dela Pierre et al., 2012; Perri et al., 2017) considered CDB as formed mainly due to microbial activity of sulfide-oxidizing bacteria like *Beggiatoa* and *Thioploca* (Guido et al., 2007), which point to a relatively deep basin typified by "normal" marine conditions in the upper layer of the water column. Sedimentological features such as brecciation, stromatolites or vuggy fabrics have been related to autobrecciation induced by the dissolution of embedded halite and gypsum (Caruso et al., 2015) or to fenestrae-like deposits linked to subaerial exposure conditions. However, these sedimentological and petrographic features are also typical of seep-carbonate deposits formed in association with chemotrophic activity of microbial mats, pervaded by intense fluid expulsion (Natalicchio et al., 2013; Himmler et al., 2022).

Recently, new petrographic and isotopic analyses on Messinian pre-evaporitic carbonates from the Tuscan-Romagna area revealed that AOM contributed to the formation of these carbonates (Conti et al., 2022), providing the unique opportunity to investigate in great detail the evolution of cold seep environment during a key transition period in Earth history which is still debated. Here, we use a multiproxy approach including field facies investigation, carbonate petrography (including optical and scanning electron microscopy), mineralogical (XRD), and isotope analyses ($\delta^{13}C$, $\delta^{18}O$) to describe for the first time seep-impacted carbonates displaying evidence of intense microbial activity sustained by methane in the Messinian pre-evaporite setting of northern Apennines.

2 Geologic setting

The Northern Apennine chain has been formed since Late Eocene-early Oligocene as a fold and thrust belt, related to the convergence between the European and African plates, with the interposition and the collision of two microplates (Corsica-Sardinia block and Adria). During the continental collision, clastic wedges accumulated in foreland basins in front of the deforming thrust belt as due to the progressive roll-back of the subducting Adriatic slab (Le Breton et al., 2017). Deposition mainly occurred in wedge-top and in foredeep basins, progressively migrating

towards NE (Argnani and Ricci Lucchi, 2001; Conti et al., 2016). The flexure of the lithosphere belonging to the Adria margin started from the most internal areas and migrated eastward through time, forming foredeep basins oriented sub-parallel to the belts and filled by large quantities of terrigenous sediments, derived from the erosion of the incipient inverted margin (orogen and former foredeep). During migration, the Apennine thrust-front incorporated foredeep siliciclastic deposits in the accretionary wedge causing the closure of the foredeep. This closure stage is marked by the deposition of slope marls with sporadic channelized sandstone bodies. The Miocene migration of the Apennine accretionary wedge was recorded by many seep-carbonate deposits rich in chemosynthetic fauna formed in correspondence of the main structural elements (Argentino et al., 2019), in spectacular outcrops of the Marnoso-arenacea Fm in the Romagna-Tuscan-Umbrian Apennines.

In the studied area (Fig. 1) the Marnoso arenacea Fm is constituted by a thick (about 3500 m) turbidite sequence of sandstone and shaly-marly layers, detached from the lower Miocene basement along a flat basal thrust and shows a deformational style dominated by fault-propagation folds forming imbricated structures (Argentino et al., 2019). During the closure stage, foredeep deposits were capped by silty-clayey hemipelagic marls with synsedimentary slide deposits and finally by sporadic diatom-rich layers and thin marls rhythmically interbedded with organic-rich mudstones informally referred as euxinic shales of the Ghioli di letto Fm (about 150 m thick). The last deposits enclose numerous seep-carbonate bodies, lens-like to stratiform, late Tortonian to early Messinian in age (Terzi et al., 1994; Conti et al., 2022). The extension of seep-carbonate bodies ranges from 1 to 100 m and the thickness varies from some decimeters to 30 m and are concentrated between the Lamone and Sintria valleys. They are in primary position, concordant with the enclosing sediments, with an Apenninic trend and moderately dipping to sub-horizontal attitudes. In the area of Parco Carnè carbonate bodies are subvertical and pass with concordant contact to the Gessoso-solfifera Fm (Montanari et al., 2007). The passage to the evaporites occurs by the interposition of about 2 m-thick laminated brownish to whitish

carbonates (Calcare di Base *auctorum*) whose genesis is still debated, object of this study. The Gessoso-solfifera Fm is made up of selenitic gypsum and clastic resedimented evaporites (Lugli et al., 2010). Gypsum beds are separated by shaly levels, suggesting cyclical pattern of deposition, and reach an overall thickness of about 200 m. Evaporites are unconformable overlaid by the Colombacci Fm (conglomerate to pelitic) followed by the Pliocene Argille Azzurre Fm. The Colombacci Fm deposited in a brackish to freshwater environment, during the final stage of the Messinian salinity crisis (Bassetti et al., 2004), in many cases with erosive contacts with the underlying evaporites or euxinic shales. The marine marls and clays of the Argille Azzurre Fm onlap the Messinian deposits recording the flooding of the Mediterranean during the early Pliocene.

3 Methods

In this study we examined six well-exposed outcrops, Cò di Sasso, M. Spugna, Case Torre, Abisso Mornig, Grotta Carnè, and Rontana (Figs. 1 and 2), where seep-carbonates concordantly pass upwards to laminated carbonate facies, and selenitic evaporites. Stratigraphic logs, from 6 to 18 m thick, were measured in detail focusing on the upper laminated facies, distinguihising lithology, fossil content, depositional and fluid-related structures. Thirty-six samples of carbonate rocks were sampled mostly from the upper laminated lithofacies (see Fig. 2 for location) for petrographic, mineralogical and isotopic analyses in order to characterize microfacies and authigenic phases. Thin sections of 20 samples were studied using a Leitz optical microscope and investigated via Scanning Electron Microscopy (SEM) hosted at the Department of Chemical and Geological Sciences, University of Modena and Reggio Emilia (Italy); semi-quantitative elemental information were acquired via energy-dispersive spectrometry (EDS) at accelerating voltage of 20 kV and spot size 60 mm. 15 standard thin sections were observed in transmitted and reflected light using a Nikon Eclipse LV100POL polarizing microscope at the Institute of Geological Sciences of the Polish Academy of Sciences (IGS PAS) in Warsaw. Some thin

sections were stained with alizarin red in order to differentiate between dolomite and $CaCO_3$ minerals under the polarizing microscope. Cathodoluminoscopy was performed using a Nikon Eclipse 80i Y-IDP polarizing microscope equipped with a CITL Mk-2 device (operating conditions: 0.003 mBar vacuum, 300 μA, 17.0 kV) also at IGS PAS. SEM was carried out on carbon-coated thin sections at the Faculty of Geology, University of Warsaw, using a FE-SEM ZEISS Sigma VP (operation conditions: 20 kV acceleration voltage, 120 μm aperture). EDS analyses were performed with two Bruker XFlash 6|10 SDD type detectors. Back-scattered electron images of microbial structures were obtained also using a Philips XL20 SEM (Thermo Fisher Scientific,Waltham, MA, USA) at 25 kV, equipped with an ECON 6 EDS detector used in conjunction with the Philips SEM, an EDX-DX4i system (Austin, TX, USA) at the Institute of Paleobiology PAS, Warsaw. Standard chemical analyses were carried out using two Bruker XFlash 6|10 EDS detectors. Optical and electron microscopic investigations on thin sections allowed in most cases to estimate the relative abundance between dolomite, calcite and aragonite. However, for some samples petrographic methods were insufficient to estimate the relative abundance of these carbonate minerals with a reasonable confidence, especially in samples containing all three carbonate phases, which were fine-crystalline and strongly intergrown with each other. Therefore, quantitative mineralogical analysis was carried out for 8 such samples using a PANalytical X'Pert PRO X-ray powder diffractometer with a Co anode and high speed linear detector PIXcel, employing the Bragg Brentano method. The samples were measured in the range 4-78˚ 2θ with a step size of 0.026˚ 2θ, in holders plowed at a speed of 1 revolution per 2 s. Fixed divergence slits 0.5˚ and Fe filter were used. Measurement time for each sample was 3 hours. The quantitative phase identification was obtained by comparing measured diffraction data to a reference database (Chung's method) using HighScore Plus software package. XRD analyses were carried out at the Faculty of Geology, University of Warsaw, Poland

Material for stable C and O isotope analysis was collected from the microcrystalline groundmass, which consists of micrite, microspar and small skeletal allochems, the latter

occurring only in the massive facies and comprising mostly foraminiferal tests plus minor share of ostracods, gastropods and bioclasts of various origin. Altogether, 30 powder samples were drilled using a hand-held dental drill and subsequently analyzed for stable C and O isotope composition in three different laboratories. All values are reported in per mil relative to V-PDB. 15 samples were reacted with 100% phosphoric acid at 70°C using a Gasbench II connected to a ThermoFisher Delta V Plus mass spectrometer at the GeoZentrum Nordbayern in Erlangen, Germany. Reproducibility and accuracy were monitored by replicate analysis of laboratory standards calibrated by assigning a $\delta^{13}C$ of +1.95‰ to NBS19 and -47.3‰ to IAEA-CO9 and a $\delta^{18}O$ of -2.20‰ to NBS19 and -23.2‰ to NBS18. Reproducibility for both $\delta^{13}C$ and $\delta^{18}O$ was better than 0.06 (1σ). Standard NBS 19 was additionally analyzed as quality control sample. 9 samples were analyzed at the Stable Isotope Laboratory of the IGS PAS using a GasBench II (Thermo Scientific) coupled to MAT 253 IRMS (Thermo Scientific) with continuous flow of He or a Thermo KIEL IV Carbonate Device coupled to a Finnigan Delta Plus isotope ratio mass spectrometer in Dual Inlet system. About 300 μg (for GasBench II) or a minimum of 20 μg of powdered sample (for KIEL IV) was reacted with anhydrous orthophosphoric acid at 70°C and the isotopic composition of released CO_2 was measured. The $\delta^{13}C$ and $\delta^{18}O$ values were calibrated with three international standards NBS 18, IAEA CO 8 and IAEA 603. Analytical precision (1σ) and reproducibility were generally better than 0.1‰ for both $\delta^{13}C$ and $\delta^{18}O$. 6 samples were analyzed at the Department of Chemical, Life and Environmental Sustainability of the University of Parma, Italy. About 10 mg were reacted with 100% phosphoric acid at 25 °C for 24 h. The purified CO_2 gas was analyzed using a Finnigan MAT 252 gas isotope ratio mass spectrometer. Analytical precision is of 0.1‰ (1σ) for both $\delta^{13}C$ and $\delta^{18}O$ values. All $\delta^{18}O$ values were corrected according to the fractionation factors and relative content of carbonate minerals present in each sample (see Table 1).

4 Results

4.1 Lithostratigraphy

The detailed stratigraphy and facies of logs are reported in Figs. 2 and 3. Seep carbonates overlie the euxinic shales of the Ghioli di letto Fm and have a variable thickness from a few decimeters to 15 m. The stratigraphic contact between the carbonates and the underlying euxinic shales is exposed in four outcrops (Cò di Sasso, Abisso Morning, Grotta Carnè and Rontana). Massive seep carbonates show the typical facies recurring in Miocene methane-derived carbonates of the Apennines (Conti et al., 2021) such as chemosynthetic fauna, breccias, veins and conduits. Chemosynthetic fauna are large, densely packed, articulated and disarticulated lucinids (Fig. 3D, E), vesicomyids and modiolid-like shells, associated with gastropods and crustaceans, In the upper portion of the massive facies small lucinids prevail with few disarticulated bathymodiolids and serpulids. Polygenic and monogenic breccias and microbreccias occur at various levels as small lenses. Massive macrofauna-rich seep carbonates pass to the transitional facies made of grey macrofauna-free carbonates with weakly pronounced or absent lamination. This passage is gradual and the transitional facies is well distinguished at the outcrop scale at Casa Torre, Mt Spugna and Grotta Carnè (Fig. 2), whereas in Abisso Mornig a sharp dissolution surface occurs at the top of the massive macrofauna-rich seep carbonates. Transitional facies was not observed at Cò di Sasso. Massive or transitional facies pass upward to white laminated, fauna-free carbonates up to 2 m thick (Fig. 3B, D). The upppermost ~60 cm of the laminated facies at Cò di Sasso is developed as stromatolitic carbonates (Fig. 3A). In all outcrops laminated carbonates are overlain by selenitic gypsum, with the exception of Casa Torre, where carbonates unconformably pass to siltstones and marl of the Colombacci Fm (Fig. 2). The contact between carbonates and gypsum is concordant and clear, in some cases marked by a selenitic gypsum with a cauliflower structure (Fig. 3C).

4.2 Mineralogy and petrography

Relative contents of carbonate minerals in all three facies obtained by petrographic (optical and electron microscopy) and mineralogical analyses (quantitative XRD) are provided in Table 1.

Dolomite, calcite and aragonite occur in highly variable contents in the massive and transitional facies. Except Cò di Sasso, the laminated facies are always dominated by dolomite, which is sometimes postdated by calcite. Aragonite is not present in the laminated facies. Carbonate material in Cò di Sasso comprises only calcite.

The massive facies (Fig. 4) in the lower part of the sections is constituted by typical seep carbonates predominantly made of primary micrite with minor early-diagenetic microspar. Micrite is composed of either calcite or dolomite, forming a homogeneous groundmass or developed as clots or peloids (Fig. 4A, C). Micritic calcite is anhedral, whereas dolomicrite is developed as planar, predominantly subhedral crystals <10 μm large, although the coarsest are < 20 μm large. Residual primary porosity exists between individual micrite crystals. Intergranular and void-filling microspar is chiefly calcitic or aragonitic and often coats micritic (both calcitic and dolomitic) allochems. Aragonite is typically developed as fibrous crystals sometimes arranged in fan-like, botryoidal aggregates. Late-diagenetic spar composed of equant calcite and dolomite is rare and never abundant. It occurs in some cavities, associated with spheroidal zoned dolomite (Fig. 4B, D). Surprisingly, pyrite, a typical mineral in seep carbonates, was rarely observed and is usually developed as small, partly oxidized framboids, more frequently observed in the laminated facies. Massive carbonates usually contain macrofauna and abundant and diversified assemblages of planktonic foraminifera (Fig. 4C).

Similar to the massive facies, the transitional facies is composed of microcrystalline micrite (clotted and peloidal) and early-diagenetic microsparite (Fig. 5A). This facies exhibits a complex carbonate mineralogy: dolomitic micrite is overgrown by acicular aragonite, followed by drusy dolomite and calcite cements (Fig. 5B, C, D). Rare detrital quartz and biotite are observed (Fig. 5B, C). Some of the cavities and intergranular pore space of transitional facies in Casa Torre are occupied by crystals of barite, as revealed by thin section and SEM-EDS analyses (Fig. 5B). Foraminifera are less abundant compared with the massive facies, chemosymbiotic macrofauna is absent, and faint lamination appears. Only small remnants of poorly preserved, reworked

fragments of hardly identifiable fossils, possibly echinoderms, bivalves and gastropods, and rare complete ostracods were observed. Large micritic grain showing concentric sparitic-micritic envelopes comprising both dolomite and aragonite, surrounded by smaller peloids and aggregates of peloids were observed in this facies (Fig. 5E, F). Some of them exhibit composite internal structure and enclose foraminiferal tests.

The carbonates in the upper laminated facies are made up of millimetre-scale alternations of dark micritic lamina alternated with microsparitic levels (Fig. 6A, C), white to gray in color and orange to yellow in CL. Neither macrofauna nor foraminifera were observed in this facies. Micritic laminae consist mainly of a dense arrangement of peloidal particles (Fig. 6B): peloids are rounded, tens of microns in size, with ovoidal to subcylindrical shape, dull luminescent. Sand- to silt-sized detrital material (quartz, K feldspar, white mica) and oxidized pyrite are rare. Locally micritic laminae show an irregular frame with a dendritic-like arrangement. Small rounded and elongated dense aggregates of dolomicrite are present with a preferred orientation parallel to the surfaces of laminae, enclosed in the microcrystalline matrix (Fig. 6C). Dark micritic laminae are alternated with gray laminae in which microspar encloses variable amounts of silica and clay particles. Larger irregular cavities and patches are also present, marked by a rim of dark dolomicrite. Void-filling spheroidal zoned dolomite is abundant in some samples representing all three facies (Figs. 4B, D and 6D, F), but is the most abundant in sample AC-12 from Casa Torre, which belongs to the laminated facies. This dolomite shows a discoidal shape with a diameter of ~100 μm (< 250 μm) and a concentric lamination associated with CL color variations between dull, orange, and yellow, which indicates that the lamination represents growth zonation. Authigenic barite was also observed in the laminated facies as < 100 μm large subhedral cavity-filling cement and < 20 μm long euhedral prismatic crystals dispersed in the matrix. Evaporative sulfate minerals occur only in the laminated facies in Cò di Sasso. They are celestine and gypsum that occur as < 0.5 mm large, anhedral, poikilotopic crystals in fine carbonate matrix (Fig. 6E). The size of these evaporitic crystals is significantly larger than that of the surrounding and

enclosed dolomite, which suggests that they precipitated post-depositionally from infiltrating saline brines related with the MSC.

4.3 Microbial content

A number of microbial fabrics are preserved in the Messinian seep-carbonates suggesting that microbial communities played a direct or indirect role in the formation of these deposits. The Casa Torre and Grotta Carnè sections displays many features of microbial sediments (Fig. 4 E, F, 5 E, F, 6 F) including irregular and wavy lamination, micritic peloids and micro-oncoidal structures occurring alternately to some extent. The microbial nature of the samples collected from laminated microfacies is manifested by the presence of structures characteristic of mineralized benthic microbial mats such as lumpy clusters of organic matter arranged in layers or larger aggregates, oncoid-like structures (Figs. 6F, 7H, I), and web-like patterns manifested in SEM after etching the rock surface with a weak HCl acid (Fig. 7 C-F). Formation of these structures, especially of the latter, requires quite fast mineralization of exopolymeric substances within the microbial mat (Kremer 2006). When mineralization of a benthic microbial mat or biofilm occurs quickly, during the life of the microorganisms forming the mat or immediately post-mortem, the spatial structure of the mat (extracellular polymeric substance EPS) is often preserved. This pattern resembles a web-like structure where pits and walls are particularly well visible on etched surfaces. Pits 5 to 20 μm in diameter seem to be remnants of degraded groups of coccoid cells that decomposed first (see degradation of cyanobacterial mat, Horodyski and Vonder Haar, 1975), where walls around pits are commonly mineralized mucilaginous sheaths secreted by microbial cells, in this case most likely unicellular coccoidal cyanobacteria, or possibly other coccoid bacteria that form mats and biofilms on the bottom and are capable of fossilization. Such structures may be visible over a large area, in the background of the rock, or only locally, depending on the degree of preservation. In the sample AC 12, a web-like microbial pattern occurs alternating with fragments where ooid/oncoid-like spherical structures occur (Fig. 6F). The peloidal micrite of samples AC11 and AC10 has some biosedimentary features

suggesting a microbial origin: the peloids with laminated and non-laminated envelopes 20 to 400 µm in diameter are a common feature (Fig. 5E, F). Some of them have a core made of micrite with a characteristic microbial pattern suggesting fossilized coccoidal cells. Elongated oval forms filled with sparite are possibly linked to burrowing. In sample AC10, among peloidal layers rod-like filaments resembling microfossils are visible (Fig. 4E,F). They occur as individuals or grouped loosely distributed within the mass of peloids. These structures are 200-500 µm long and 40-60 µm wide. The width of individual filament is more or less uniform along its length. Their shapes are mostly straight or only slightly curved.

In the laminated deposits of Cò di Sasso section, indicative features of microbial activity include the presence of filamentous microfossils (up to 400 µm long and about 50 µm wide) with an elongated shapes, usually chaotically arranged. Similar short filaments are also present in Abisso Moning and Casa Torre sections, but they are not well preserved. Clotted micrite microfabrics and peloids are frequent forming micritic laminae and horizontally elongated fenestrae. Peloids form aggregates resembling grapestones. Micritic peloids are apparently overgrown by sparitic envelops.

4.4 Stable oxygen and carbon isotope composition

The C and O isotopic composition is similar in three sections: Casa Torre, Abisso Mornig, and Grotta Carnè represented by 23 samples (Table 1, Fig. 8). They exhibit very depleted $\delta^{13}C$ values from -51.2 to -25.2‰ (generally lower than those recorded in other Miocene seep-carbonates of the northern Apennines) with one outlier of -14.4‰ for specimen AC11 representing the transitional facies (average = -39.7‰, sd 8.6‰). Their $\delta^{18}O$ values are mostly positive, from -0.3 to +5.2‰, with four outliers of -5.3, -4.2, -2.7 and -2.5‰ for specimens from Abisso Mornig 36A, 36Ca, 36B and Casa Torre AC9, respectively (average = +1.8‰, sd 3.0). No appreciable differences exist in $\delta^{13}C$ values between the facies distinguished, whereas $\delta^{18}O$ values appear to be higher in the laminated facies, where they do not drop below +4.1‰. On average, the $\delta^{18}O$ values rise and become more uniform from the massive (average = +0.1‰, sd = 3.0‰, n = 11),

through transitional (+2.0, sd = 2.6, *n* = 6), to the laminated facies (+4.6‰, sd = 0.4‰, *n* = 6). In Cò di Sasso, the only sample representing the massive facies has a similar isotope composition to those in other sections, with depleted $\delta^{13}C$ = -22.4‰ and neutral $\delta^{18}O$ = +0.1‰, whereas the isotopic composition of the six calcitic samples representing laminated facies is completely different with respect to those from the other three sections dominated by dolomite. They show much higher, uniform, although still negative $\delta^{18}O$ values from -7.4 to -6.1‰ (average = -6.9‰, sd = 0.5‰) and less depleted values $\delta^{13}C$ from -12.4 to -6.3‰ (average = -9.5‰, sd = 2.6‰).

5 Discussion

The studied outcrops of Messinian carbonates in the Tuscan-Romagna area share a common upward stratigraphic trend: massive seep carbonates rich in large lucinids and modiolids show a progressive decrease in the size of chemosymbiotic invertebrates replaced by small lucinids and serpulids and invariably pass upward to laminated carbonates with the interposition of a macrofauna-free transitional facies. The microcrystalline groundmass in all samples is mostly composed of primary micrite, both calcitic and dolomitic, with preserved primary porosity, which is partly filled with early-diagenetic microspar cements of calcitic and aragonitic mineralogy. Therefore, studied carbonates are penecontemporaneous precipitates that constitute an archive of basin- and shallow pore-water. The laminated deposits are mostly composed of dolomicrite microlaminae rich in peloidal particles alternated with microsparitic calcite layers including scarce amounts of clay minerals. It appears that the deposition was controlled or influenced by a number of factors such as methane release, microbial activity, variation in salinity, redox conditions, and depth, as discussed below.

5.1 Methane-related origin of carbonates

In methane-rich environments, AOM performed by methanotrophic archaea in syntrophic partnership with sulfate-reducing bacteria (Boetius et al., 2000) is an important source of isotopically depleted DIC to the shallow pore waters, leading to precipitation of carbonates with

$\delta^{13}C$ < -30‰. The samples from our study showed $\delta^{13}C$ values as low as -54.3‰ which is the most negative value ever reported from Messinian pre-evaporitic carbonates in Italy and most of our samples across the outcrops are lighter than -35‰. These values clearly indicate variable amounts of incorporation of methane-derived carbon thus confirming a methane-charged sedimentary setting. These isotopic values may also suggest that the methane source feeding AOM at the study site had a significant microbial gas component shifting $\delta^{13}C$ values toward < -50‰ (Milkov and Etiope, 2018). Microbial mats are known to thrive at modern cold seeps, inhabiting the sites with the highest methane fluxes (Argentino et al., 2022) and are often associated with carbonate precipitation induced by AOM in the shallow subsurface. The fossilization of microbial mats requires prolonged and intense AOM inducing carbonate supersaturation and rapid carbonate precipitation close to the seafloor (Peckmann et al., 2004). Due to the ephemeral and dynamic nature of cold seeps, the observation of modern stromatolite - like carbonate deposits at active marine seeps is quite rare (Bailey et al., 2009; Himmler et al., 2018) compared to ancient long-lived systems exposed on land, as reported in our study.

In our study, despite the strong isotopic evidence for methane oxidation, it is difficult to unequivocally demonstrate that methane discharge reached the water column. However, the combined evidence of very intense methane oxidation at or near the seafloor provided by isotopic, petrographic and mineralogical data seems to support that interpretation. It is very likely that a fraction of the upward migrating methane escaped the AOM biofilter in the sediment and was eventually vented into the water column (Stranne et al., 2022).

SEM-EDS microanalyses detected authigenic barite developed either as < 20 μm long euhedral prismatic crystals in the matrix, < 100 μm subhedral cavity-filling crystals (Figs. 4F and 5B), or microcrystalline anhedral intergranular cement (Fig. 5B). Barite enrichments in seep-impacted sediment can be associated with the formation of barite fronts at the top of the SMTZ, where sulfate encounters Ba-rich pore waters rising from the underlying anoxic sedimentary interval (Torres et al., 1996; Carter et al., 2020). Long-time stabilization of the SMTZ at a certain depth

creates especially favorable conditions for such diagenetic barite precipitation (Bojanowski et al., 2019). However, in our case, the striking co-occurrence of barite crystals in microbially-derived laminae make us propend for an origin related to remineralization of organic-rich layers, during which fresh sedimentary organic matter released Ba^{2+} and induced supersaturated conditions within microenvironments, causing barite precipitation (Carter et al., 2020).

5.2 Microbial origin of laminated carbonates: taxonomic affiliation

The studied Messinian seep-carbonates contain several structures typical of microbial sediments, such as laminations, peloids, filamentous forms, clotted micrite, fibrous and botryoidal aragonite cement, and frequent fenestrae. The remnants of filamentous microorganisms are preserved in the peloid-rich transitional and laminated facies. Establishing the taxonomic affiliation of these forms is difficult: the threads are rare and mixed with peloids. However, the relatively large size of the threads suggests their cyanobacterial (or some other bacterial) or algal origin. Both cyanobacteria and single-celled filamentous algae can form mats made of networks of benthic or planktonic microorganisms. The individual filament accumulation does not give a clear indication of whether it is the remains of fallen plankton or a benthic mat.

The affiliation of similar filamentous forms is discussed in the literature concerning the Messinian deposits. These forms have been interpreted as the remains of benthic algae (Vai and Ricci Lucchi, 1977), cyanobacteria (Rouchy and Monty, 2000) or sulfide-oxidizing bacteria (Dela Pierre et al., 2015). The presence of sulfur bacteria has been already observed in modern and ancient seep-associated environments. Peckmann et al. (2004) interpret thread-like forms from an adjacent outcrop of massive seep carbonates at Pietralunga as colorless sulfur bacteria. Their interpretation is based on similarity to the modern filamentous sulfur bacterium *Thioploca* (Jørgensen et al., 2010). Taxonomic identification is, however, difficult due to the morphological similarity between cyanobacteria and sulfur-oxidizing bacteria (Bailey et al. 2009). Similar to the examined deposits are also stromatolites from the Lower Messinian of the Calcare di Base Fm

from Sicily (Oliveri et al., 2010). The dominant microstructures of these stromatolites are peloids and clotted fabrics, bacterial-like microfilaments and micrites with fenestral structures. Based on morphology, the filaments have been interpreted as *Beggiatoa*-like sulpur bacteria, although some of the larger cyanobacteria, e.g. *Scytonema*, might be similar in filament size (Oliveri et al 2010).

The "web structures" are typical of mat-forming coccoid cyanobacteria (see Horodyski and Vonder Haar, 1975; Kaźmierczak et al., 1996). The web-like pattern in the Casa Torre section visible in SEM images (Fig. 7A-G) is comparable to structures known both from modern and fossil benthic coccoidal cyanobacterial mats that underwent early mineralization (Kempe and Kaźmierczak, 1993) such as cyanobacterial mats from Sulejów Dam, Poland, and subfossil mats from a crater lake on Satonda Island, Indonesia (Fig. 7 J-K). In both cases cyanobacterial mats were mineralized with calcium carbonate. It is well known that cyanobacteria may trigger carbonate mineralization reactions by increasing the saturation state within the exopolymeric substances (e.g. Jansson and Northen, 2010). Most likely the web-like structures from Messinian sediments are just remnants of cyanobacterial mats, resemble *Entophysalidaceae* or other coccoidal cyanobacteria, thriving at the bottom of the Messinian sea. They co-occur with oncoid-like forms, whose microbial origins are commonly accepted and that confirm participation of microorganisms in the formation of these deposits (for review see Peryt, 1981). Peloids have been suggested to be a product of bacterially induced carbonate precipitation (Chafetz, 1986; Buczynski and Chafetz, 1983; Kaźmierczak et al., 1996). This microbial assemblage, composed mainly of coccoidal cyanobacterial mats and other bacteria that commonly co-exist with cyanobacteria, differs from the laminated peloid-rich carbonates with filaments known from the Cò di Sasso and Abisso Mornig sections dominated by benthic microbial mats composed most likely of filamentous organisms.

5.3 Environmental insights

Both green algae and cyanobacteria require a photic zone habit. In terms of bathymetry, the depth of such a zone varies and is related to water transparency which depends on many factors, such as plankton blooms in the water column or suspended clay content. However, it is agreed that the mesophotic zone reaches ca. 150 m water depth in tropical and subtropical regions (Lesser et al., 2009). Cyanobacteria are known to maintain active photosynthesis at low irradiance levels (Jodłowska and Śliwińska, 2014) and therefore can live well at a depth of 200 m where low-light conditions dominate (Kremer and Kaźmierczak, 2005). Because sulfur oxidizing bacteria are known to occur in a wide range of water depth they are rather poor bathymetry indicators. They, however, live in oxygen-poor and nitrate-rich waters such as documented for *Thioploca* (Jørgensen and Gallardo, 1999).

In the studied sections, especially in Cò di Sasso and Abisso Mornig, a sequence is noticeable from the bottom to the top of evidently marine sediments with marine fauna, e.g. foraminifera, bivalve mollusks and serpulid tube worms, through laminated microbialite facies without macrofauna, to gypsum. Such a succession is consistent with a gradual increase in salinity; microbial-cyanobacterial facies are commonly associated with conditions of elevated salinity intolerable by other organisms. As discussed by Georgieva et al. (2019), aggregation of serpulid tubes is common in cold seeps and may be particularly intensive as a result of sea-level lowstand.

Although there is no conclusive paleobiological evidence for the elevated salinity, the Messinian microbialites herein analyzed can be compared to similar modern deposits from environments of higher salinity. The bottom of the lake Big Pond (Eleuthera, Bahamas), showing salinity ranging from 80 to 240 g/l, is covered with extensive cyanobacterial mats within which EPS carbonate minerals precipitate. Similarly to the Messinian carbonates, typical microbial microstructures, such as micropeloids, fenestral pores, fibrous cements and aggregates of peloids, have been observed in the deposits of the Bahamian mats (Glunk et al., 2011). Therefore, based on facies similarity, it can be suggested that the Messinian microbialites were deposited in a similar environment of increased salinity. A similar interpretation may be suggested based on the

similarity of these sediments to the Messinian deposits in Sicily (Calcare di Base Fm) where alternations of dense micrite and peloidal laminae, clotted micrite, frequent fenestrae and short microbial filaments occur. Shallow hypersaline marine conditions with microbial assemblages composed of sulfur and sulfate-reducing bacteria have been proposed for these sediments in Sicily (Oliveri et al., 2010).

About paleodepth, we do not have clear indications to estimate depositional depth, as the observed sedimentary structures can be found in a wide range of settings from deep to very shallow. A useful constrain may be provided by the estimate depth for selenitic gypsum overlying the laminated carbonates in stratigraphic concordance. Lugli et al. (2010) argue that lower gypsum deposited in restricted marginal basins less than 200 m deep, while no gypsum could precipitate in the deeper euxinic settings.

5.4 Paleoenvironmental interpretation of carbon and oxygen isotope data

We have attempted to estimate $\delta^{18}O$ of the parent fluid for the samples analyzed with the following assumptions. As we have no clear evidence of features usually indicative of gas hydrate dissociation in northern Apennine paleoseeps, such as spongy or vuggy fabric, we consider doubtful that ^{18}O enrichment is related to the destabilization of gas hydrates. Moreover, the basin was rather too shallow, given the moderate paleolatitude and warm climate conditions, for hydrates to develop. The water depth was ~200 m, as constrained by the presence of mat requiring the photic zone (see above) on one side and by the depth of the basin investigated during the onset of the MSC, when the overlying gypsum evaporites were deposited (Lugli et al., 2010) on the other.

Surface water temperature between 19.5 and 27.5°C was estimated for the Mediterranean sea at the onset of the MSC (Kontakiotis et al., 2022). For our calculations, we need to use bottom water temperature, as the microcrystalline groundmass of both massive seep carbonates and dolomitic laminated microbialites formed at or slightly below the sediment-water interface. A

minor influence from the photic zone may only be taken into consideration for the massive facies rich in planktonic foraminifera. Still, this influence is considered as negligible due to the overwhelming dominance of microcrystalline cements. Bottom water temperature data for the Mediterranean Sea at the onset of the MSC are not available, so we need to base our assumptions on indirect data. Since surface water temperature and maximum depth in modern Adriatic Sea could be similar to those estimated for the Mediterranean during the onset of the MSC, we use the data from the Adriatic in our estimation. Thus, we use the current bottom water temperature in the Adriatic Sea at 200-250 m water depth of ~11°C (Marini et al., 2006). Given this temperature, the $\delta^{18}O$ values measured for the microcrystalline carbonate samples, the 2.6‰ offset in $\delta^{18}O$ values between dolomite and calcite precipitated at the same temperature (Vasconcelos et al., 2005), and the estimation of relative content of carbonate phases in the carbonate fraction (Table 1), we calculated $\delta^{18}O$ values of the parent fluid ($\delta^{18}O_{water}$) from -8.7 to +2.3‰ SMOW (Table 1) by application of paleotemperature equation for calcite of Anderson and Arthur (1983):

$$T\ (°C) = 16.0 - 4.14(\delta^{18}O_{carb} - \delta^{18}O_{water}) + 0.13(\delta^{18}O_{carb} - \delta^{18}O_{water})^2.$$

The $\delta^{18}O$ values of the parent fluid in Casa Torre, Abisso Mornig, and Grotta Carnè are mostly within the ranges for coeval Mediterranean and ocean water (Paul et al., 2001; Rigaudier et al., 2011). Values obtained for the laminated facies in Cò di Sasso are significantly lower possibly indicating a meteoric influence, further supported by their moderately depleted $\delta^{13}C$ values.

Consistent differences in $\delta^{18}O$ values of the parent fluid are observed between the facies for Casa Torre, Abisso Mornig, and Grotta Carnè, although with overlaps (Fig. 9). These values vary in a broad range between -6.6 and -0.1‰ (median = -1.6‰, sd = 2.2‰, *n* = 11) for the massive facies, between -4.0 and +2.3‰ (median = -0.1‰, sd = 2.2‰, *n* = 6) for the transitional, but are always positive between +0.3 and +1.6‰ (median = 1.1‰, sd = 0.5‰, *n* = 6) for the laminated facies. Thus, they rise from the massive, through transitional, to the laminated microbialite facies in these sections. Such tendency could indicate either a drop of bottom-water temperature or a rise of salinity at the transition from the massive to laminated facies. The median values of the

calculated parent fluid $\delta^{18}O$ rise by 2.7‰ from the massive to laminated facies. Assuming constant temperature, this would be translated to 6-13 p.s.u. (practical salinity unit) rise by taking current $\delta^{18}O$-salinity relationships from different parts of the Mediterranean basin that range from 0.199 to 0.48 $\delta^{18}O$/p.s.u (see Kontakiotis et al., 2022 and references therein). Assuming ice-free world, constant and normal marine salinity, this would be translated to a ~11°C temperature decrease, which is unlikely given the paleogeographic and climatic setting of the Mediterranean and the obvious evaporitic deposition during the MSC.

In summary, in sections Casa Torre, Abisso Mornig, and Grotta Carnè, a distinctive depositional and biotic switch is observed from massive seep carbonates to laminated microbialite facies reflecting important environmental changes taking place in the basin. This switch is associated with abrupt disappearance of macrofauna and planktonic foraminifera, predominance of dolomite over calcite, absence of aragonite. Evidently, temperature drop may not have been the main driver of this change and salinity increase appears to have played the major role. However, the magnitude of ~10 p.s.u. of salinity rise appears to be too modest to fully explain the change as well, especially that primary evaporitic sulfate minerals have not been observed in these carbonates. Thus, another paleoenvironmental change must have co-occurred in order to account for the dramatic shift observed.

We found considerable differences in the laminated facies between Cò di Sasso and the other sections investigated, namely much higher $\delta^{13}C$, much lower $\delta^{18}O$, calcitic mineralogy, and presence of post-depositional evaporitic sulfates in the earlier. Despite these differences, microfacies characteristics in the laminated facies are the same in Cò di Sasso as in other sections, all representing laminated microbialites. The $\delta^{18}O$ values of the laminated facies in Cò di Sasso are strongly depleted (median = -8.3‰, sd = 0.5‰, n = 6) and much lower than in other sections studied. It could be that Cò di Sasso has experienced different alteration and was affected by meteoric diagenesis later in the history of that outcrop. However, we have not observed clear petrographic effects of significant postdepositional alteration. Moreover, the $\delta^{13}C$ are by 20-40‰

higher than those of the laminated facies in other outcrops, which cannot be explained by postdepositional alteration, because C isotopes are relatively insensitive to resetting during diagenesis and retain the isotopic composition of the precursor even during burial recrystallization (Bojanowski et al., 2014). Therefore, the isotopic composition of carbonates from Cò di Sasso should be interpreted with respect to the paleoenvironment.

We propose a possible scenario explaining all these data together for all sections examined. The paleoenvironmental model is analogous to that proposed by Bojanowski et al. (2018) for the Central Paratethys, minding that it is partly speculative, as it lacks a solid evidence in some points. Further research is surely needed to investigate applicability of this model to the Mediterranean shortly before the MSC in detail. The drastic changes recorded in the sections examined can be explained by the development of water-column stratification with respect to both salinity and oxygen concentration during the restriction of the Mediterranean Sea preceding the Messinian Salinity Crisis. Cò di Sasso represents a proximal, shallow water environment that became strongly influenced by riverine flux during the deposition of the laminated facies. It resulted in the increase of $\delta^{13}C$ probably related to termination of the gas source sustaining the anaerobic oxidation of methane and a switch to dominance of soil-derived dissolved inorganic carbon (DIC) supplied by the riverine flux. Considerable riverine discharge was also responsible for the decrease of $\delta^{18}O$ values in the laminated calcitic facies having C and O isotope composition in fact typical for a freshwater environment. In the remaining sections, where the environment was more distal, AOM continued and dolomite was forming at or slightly below the sediment-water interface, so that dolomite $\delta^{18}O$ reflects conditions and O isotope composition of the deep bottom water. The reason is that the basinal parts became covered by anoxic, saline bottom water, which allowed for a continued anaerobic oxidation of methane, but without the involvement of chemosymbiotic macrofauna, which is unable to survive in oxygen-free environments. Planktonic foraminifera disappeared in the laminated facies, because salinity in the

photic zone was probably too low due to the widespread dispersion of fresh water in the surface layer.

6 Conclusions

The Upper Miocene carbonate succession preceding the Messinian evaporites in the northern Apennines recorded the transition from marine to evaporitic conditions which eventually led to the widespread deposition of hundred-meter thick gypsum in large areas of the Mediterranean basin. The passage to the overlying evaporites is marked by the occurrence of microbially-precipitated laminated carbonates consistent with precipitation induced by anaerobic oxidation of methane with depleted $\delta^{13}C$ values indicating incorporation of methane-derived carbon. The web-like structures in laminated carbonates are remnants of cyanobacterial mats, resembling *Entophysalidaceae* or other coccoidal cyanobacteria, thriving at the bottom of the Messinian sea. They co-occur with oncoid-like forms and benthic microbial mats.

The transition from massive seep to laminated carbonates is associated with an abrupt loss of macrofauna and planktonic foraminifera, predominance of dolomite over calcite, and an increase of $\delta^{18}O$ values. These remarkable depositional and geochemical changes reflect an important environmental shift. Although there is no conclusive paleobiological evidence for the elevated salinity, the Messinian microbialites can be compared to similar modern deposits from environments of higher salinity. The $\delta^{18}O$ data confirms that this depositional switch was associated with a bottom-water salinity rise. However, salinity fluctuations seem insufficient to explain all the depositional changes, so they must have been accompanied by other environmental factors. We propose that water-column stratification with respect to both salinity and oxygen concentration developed in the Mediterranean basin, recorded by the transition from massive, macrofauna-rich seep to laminated microbialite carbonate facies. This hypothesis is potentially important to better understand the full spectrum of environmental changes occurring shortly before the Messinian salinity crisis. Our data improve also the comprehension of processes of

methane oxidation and MDAC formation at cold seeps, especially with respect to their response to environmental evolution from normal marine to higher-salinity stressed conditions.

Acknowledgments

The work was funded by the Polish National Science Centre grant no. 2020/37/B/ST10/01769, and by Far Unimore 2023. We are grateful to the Editor, to J.M. Soria and the anonymous reviewers for the accurate and precise revisions that greatly improved the manuscript. We are indebted to Andreas Wetzel for discussion and suggestions in the field and to Paolo Serventi for assistance in sampling and lab.

References

Agirrezabala, L.M., Kiel, S., Blumenberg, M., Schäfer, N., and Reitner, J., 2013. Outcrop analogues of pockmarks and associated methane-seep carbonates: A case study from the Lower Cretaceous (Albian) of the Basque-Cantabrian Basin, western Pyrenees. Palaeogeography, Palaeoclimatology, Palaeoecology, 390, 94–115.

Anderson, T.F., Arthur, M.A., 1983. Stable isotopes of oxygen and carbon and their application to sedimentologic and paleoenvironmental problems. In: Stable Isotopes in Sedimentary Geology, Society of Economic Paleontology and Mineralogy, Short Course 10, Section 1.1-1.151.

Argentino, C., Conti, S., Crutchley, G.J., Fioroni, C., Fontana, D., Johnson, J.E., 2019. Methane-derived authigenic carbonates on accretionary ridges: Miocene case studies in the northern Apennines (Italy) compared with modern submarine counterparts. Marine and Petroleum Geology 102, 860–872.

Argentino, C., Johnson, J. E., Conti, S., Fioroni, C., Fontana, D., 2020. Preservation of ^{34}S-enriched sulfides in fossil sulfate-methane transition zones: new evidence from Miocene outcrops of the northern Apennines (Italy). Geo-Marine Letters, 40, 379–390.

Argentino, C., Savini, A., Panieri, G., 2022. Integrating Fine-Scale Habitat Mapping and Pore

Water Analysis in Cold Seep Research: A Case Study from the SW Barents Sea. In: World Atlas of Submarine Gas Hydrates in Continental Margins, Cham. Springer International Publishing 505–514, doi:10.1007/978-3-030-81186-0_43.

Argnani, A., Ricci, Lucchi F., 2001. Tertiary siliciclastic turbidite systems of the Northern Apennines. In: Vai, G.B., Martini, I.P. (Eds.), Anatomy of a Mountain: The Apennines and Adjacent Mediterranean Basins. Kluwer Academic Publisher, London, 327–350.

Bailey, J.V., Orphan, V.J., Jove, S.B., Corsetti F.A., 2009. Chemotrophic Microbial Mats and Their Potential for Preservation in the Rock Record. Astrobiology, 9, 1–17.

Bassetti, M.A., Manzi, V., Lugli, S., Roveri, M., Longinelli, A., Ricci Lucchi, F., Barbieri, M., 2004. Paleoenvironmental significance of Messinian post-evaporitic lacustrine carbonates in the northern Apennines, Italy. Sedimentary Geology, 172, 1–18.

Birgel, D., Guido, A., Liu, X., Hinrichs, K.U., Gier, S., Peckmann, J., 2014. Hypersaline conditions during deposition of the Calcare di Base revealed from archaeal di- and tetraether inventories. Organic Geochemistry, 77, 11–21.

Boetius, A., Ravenschlag, K., Schubert, C.J., Rickert, D., Widdel, F., Gieseke, A., Amann, R., Jørgensen, B.B., Witte, U., Pfannkuche, O., 2000. A marine microbial consortium apparently mediating anaerobic oxidation of methane. Nature, 407, 623–626.

Bojanowski, M.J., Barczuk, A., Wetzel, A., 2014. Deep-burial alteration of early-diagenetic carbonate concretions formed in Paleozoic deep-marine greywackes and mudstones (Bardo Unit, Sudetes Mts., Poland). Sedimentology, 61, 1211–1239.

Bojanowski, M. J., Ciurej, A., Haczewski, G., Jokubauskas, P., Schouten, S., Tyszka, J., & Bijl, P. K. (2018). The Central Paratethys during Oligocene as an ancient counterpart of the present-day Black Sea: Unique records from the coccolith limestones. Marine Geology, 403, 301–328.

Bojanowski, M.J., Kędzior, A., Porębski, S. J., and Radzikowska, M., 2019, Origin and significance of early-diagenetic calcite concretions and barite from Silurian black shales in the East European Craton, Poland. Acta Geologica Polonica, 69, 403–430.

Bojanowski, M.J., Oszczypko-Clowes, M., Barski, M., Oszczypko, N., Radzikowska, M., Ciesielska, Z., 2021. Slope destabilization provoked by dissociation of gas hydrates in the Outer Carpathian basin during the Oligocene: Sedimentological, petrographic, isotopic and biostratigraphic record. Marine and Petroleum Geology, 123, 104585.

Borrelli, M., Perri, E., Critelli, S., Gindre-Chanu, l., 2021. The onset of the Messinian Salinity Crisis in the central Mediterranean recorded by pre-salt carbonate/evaporite deposition**.** Sedimentology, 68, 1159–1197.

Buczynski, C., Chafetz, H.S., 1993. Habit of bacterially induced precipitates of calcium carbonate. In: Rezak, R., Lavoie, D.L. (Eds.), Carbonate Microfabrics, Springer, New York, pp. 105–116.

Cao, H., Zhang, W., Wang, Y., Qian, P.Y., 2015. Microbial community changes along the active seepage site of one cold seep in the Red Sea. Frontiers in Microbiology, 6, doi:10.3389/fmicb.2015.00739.

Carter, S.C., Paytan, A., Griffith, E.M., 2020. Toward an improved understanding of the marine barium cycle and the application of marine barite as a paleoproductivity proxy. Minerals, 10, 1–24.

Caruso, A., Pierre, C., Blanc-Valleron, M.M., Rouchy, J.M., 2015. Carbonate deposition and diagenesis in evaporitic environments: The evaporative and sulphur-bearing limestones during the settlement of the Messinian Salinity Crisis in Sicily and Calabria. Palaeogeography, Palaeoclimatology, Palaeoecology, 429, 136–162.

Chafetz, H.S., 1986. Marine peloids: a product of bacterially induced precipitation of calcite. Journal of Sedimentary Research, 56, 812–817.

Cochran, J.K., Landman, N.H., Jakubowicz, M., Brezina, J., Naujokaityte, J., Rashkova, A., Garb, M.P., Larson, N.L., 2022. Geochemistry of Cold Hydrocarbon Seeps: An Overview. In: Kaim, A., Cochran, J.K., Landman, N.H. (Eds.), Ancient hydrocarbon seeps. Topics in Geobiology 50, chapter 1, Springer, New York.

Conti, S., Fontana, D., Lucente, C.C., 2008. Authigenic seep-carbonates cementing coarse-grained deposits in a fan-delta depositional system (middle Miocene, Marnoso-arenacea Formation, central Italy). Sedimentology, 55, 471–486.

Conti, S., Fontana, D., Lucente, C.C., Pini, G.A., 2014. Relationships between seep-carbonates, mud volcanism and basin geometry in the Late Miocene of the northern Apennines of Italy: the Montardone mélange. International Journal of Earth Sciences, 103, 281–295.

Conti, S, Fioroni, C., Fontana, D., Grillenzoni, C., 2016. Depositional history of the Epiligurian wedge-top basin in the Val Marecchia area (northern Apennines, Italy): a revision of the Burdigalian-Tortonian succession. Italian Journal of Geosciences, 135, 324–335.

Conti, S., Fioroni, C., Serventi, P., Fontana, D., 2022. Messinian seep-carbonates marking the transition to the evaporite deposits in the Romagna sector of the northern Apennines (Italy). Italian Journal of Geosciences, 141, 350–362.

Cosentino, D., Buchwaldt, R., Sampalmieri, G., Iadanza, A., Cipollari, P., Schildgen, T.F., Hinnow, L.A., Ramezani, J., Bowring, S.A., 2013. Refining the Mediterranean “Messinian Gap” with high precision U-Pb zircon geochronology, central and northern Italy. Geology, 41, 323–326.

Crémière, A., Lepland, A., Chand, S., Sahy, D., Condon, D.J., Noble, S.R., Martma, T., Thorsnes, T., Sauer, S., Brunstad, H., 2016. Timescales of methane seepage on the Norwegian margin following collapse of the Scandinavian Ice Sheet. Nature Communications, 7, 1–10.

Dela Pierre, F., Clari, P., Bernardi, E., Natalicchio, M., Costa, E., Cavagna, S., Lozar, F., Lugli, S., Manzi, V., Roveri, M., Violanti, D., 2012. Messinian carbonate-rich beds of the Tertiary Piedmont Basin (NW Italy): Microbially-mediated products straddling the onset of the salinity crisis. Palaeogeography, Palaeoclimatology, Palaeoecology, 344-345, 78–93.

Dela Pierre, F., Natalicchio, M., Ferrando, S., Giustetto, R., Birgel, D., Carnevale, G., Gier, S., Lozar, F., Marabello, D., Peckmann, J., 2015. Are the large filamentous microfossils preserved in Messinian gypsum colorless sulfide-oxidizing bacteria? Geology, 43(10), 855–858. doi: https://doi.org/10.1130/G37018.1

Dreier, A., Hoppert, M., 2014. Following the traces of symbiont bearing molluscs during earth history. Gottingen Contributions to Geosiences, 77, 83–97.

Dubilier, N., Bergin, C., Lott, C., 2008. Symbiotic diversity in marine animals: the art of harnessing chemosynthesis. Nature Reviews Microbiology, 6, 725–740.

Feng, D., Chen, D., Peckmann, J., 2009. Rare earth elements in seep carbonates as tracers of variable redox conditions at ancient hydrocarbon seeps. Terra Nova, 21, 49–56.

Fischer, D., Sahling, H., Nöthen, K., Bohrmann, G., Zabel, M., Kasten, S., 2012. Interaction between hydrocarbon seepage, chemosynthetic communities, and bottom water redox at cold seeps of the Makran accretionary prism: Insights from habitat-specific pore water sampling and modeling. Biogeosciences 9, 2013–2031.

Fossing, H., Gallardo, V.A., Jorgensen, B., Huttel, M., Nielsen, L.P., Schulz, H., Canfield, D.E., Forster, S., Glud, R.N., Ramsing, N.B., Teske, A., B., Ulloa, U., 1995. Concentration and transport of nitrate by the mat-forming sulphur bacterium Thioploca. Nature, 374, 713-715.

García-Veigas, J, Gibert, L, Cendón, DI, et al., 2020. Late Miocene evaporite geochemistry of Lorca and Fortuna basins (Eastern Betics, SE Spain): Evidence of restriction and continentalization. Basin Research, 32, 916–948. https://doi.org/10.1111/bre.12408

Georgieva, M.N., Paull, C.K., Little, C.T.S., McGann, M., Sahy, D., Condon, D., Lundsten, L., Pewsey, J., Caress, D.W., Vrijenhoek R.C., 2019. Discovery of an extensive deep-sea fossil Serpulid Reef associated with a cold seep, Santa Monica Basin, California. Frontiers in Marine Sciences, 6, 1–18.

Glunk, C., Dupraz, C., Braissant, O., Gallagher, K.L., Verrecchia, E.P., Visscher, P.T., 2011. Microbially mediated carbonate precipitation in a hypersaline lake, Big Pond (Eleuthera, Bahamas). Sedimentology, 58, 720–738.

Grünke, S., Lichtschlag, A., de Beer, D., Felden, J., Salman, V., Ramette, A., Schulz-Vogt, H.N., Boetius, A., 2012. Mats of psychrophilic thiotrophic bacteria associated with cold seeps of the Barents Sea. Biogeosciences, 9(8), 2947–2960.

Guido, A., Jacob, J., Gautret, P., Laggoun-Défarge, F., Mastandrea, A., Russo, F., 2007. Molecular fossils and other organic markers as palaeoenvironmental indicators of the Messinian Calcare di Base Formation: normal versus stressed marine deposition (Rossano Basin, northern Calabria, Italy). Palaeogeography, Palaeoclimatology, Palaeoecology, 255, 265–283.

Himmler, T., Smrzka, D., Zwicker, J., Kasten, S., Shapiro, R.S., Bohrmann, G., Peckmann, J., 2018. Stromatolites below the photic zone in the northern Arabian Sea formed by calcifying chemotrophic microbial mats. Geology, 46, 339–342.

Himmler, T., Crémière, A., Birgel, D., Wirth, R., Orphan, V.J., Kirsimäe, K., Knies, J., Peckmann, J., Lepland, A., 2022. Putative fossils of chemotrophic microbes preserved in seep carbonates from Vestnesa Ridge, off northwest Svalbard, Norway. Geology, 50, 169–173.

Horodyski, R. J., Vonder Haar, S. P., 1975. Recent calcareous stromatolites from Laguna Mormona (Baja California), Mexico. Journal of Sedimentary Research, 45(4): 894–906. doi: https://doi.org/10.1306/212F6E7E-2B24-11D7-8648000102C1865D.

Hsu, K.J., Ryan, W.F.B., Cita, M.B., 1973. Late Miocene dessiccation of the Mediterranean. Nature, 242, 240–244.

Hu, Y., Feng, D., Peckmann, J., Roberts, H.H., Chen, D., 2014. New insights into cerium anomalies and mechanisms of trace metal enrichment in authigenic carbonate from hydrocarbon seeps. Chemical Geology, 381, 55–66.

Jansson, C., Northen, T., 2010. Calcifying cyanobacteria – the potential of biomineralization for carbon capture and storage. Current Opinion in Biotechnology, 21(3), 365–371.

Jodłowska, S., Śliwińska, S., 2014. Effects of light intensity and temperature on the photosynthetic irradiance response curves and chlorophyll fluorescence in three picocyanobacterial strains of Synechococcus. Photosynthetica, 52, 223–232.

Jørgensen, B.B., Gallardo, V.A., 1999. *Thioploca* spp.: filamentous sulfur bacteria with nitrate vacuoles. FEMS Microbiology Ecology, 28(4), 301–313. https://doi.org/10.1111/j.1574-6941.1999.tb00585.x.

Jørgensen, B.B., Dunker, R., Grünke, S., Røy, H., 2010. Filamentous sulfur bacteria, *Beggiatoa* spp., in arctic marine sediments (Svalbard, 79°N). FEMS Microbiology Ecology, 73, 500–513.

Joye, S.B., 2020. The Geology and Biogeochemistry of Hydrocarbon Seeps. Annual Review of Earth and Planetary Sciences, 48, 205–231.

Judd, A.G., Hovland, M., 2007. Seabed fluid flow: the impact of geology, biology and the marine environment. Cambridge University Press, 442 pp.

Judd, A., Noble-James, T., Golding, N., Eggett, A., Diesing, M., Clare, D., Silburn, B., Duncan, G., Field, L., Milodowski, A., 2020. The Croker Carbonate Slabs: extensive methane-derived authigenic carbonate in the Irish Sea—nature, origin, longevity and environmental significance. Geo-Marine Letters, 40, 423–438.

Kalanetra, K.M., Joye, S.B., Sunseri, N.R., Nelson, D.C., 2005. Novel vacuolate sulfur bacteria from the Gulf of Mexico reproduce by reductive division in three dimensions. Environmental Microbiology, 7, 1451–1460.

Kaźmierczak, J., Coleman, M., Gruszczyński, M., Kempe, S., 1996. Cyanobacterial key to the genesis of micritic and peloidal limestones in ancient seas. Acta Palaeontologica Polonica, 41, 319–338.

Kempe, S., Kaźmierczak, J., 1993. Satonda Crater Lake, Indonesia: Hydrogeochemistry and bio-carbonates. Facies, 28, 1–32.

Kontakiotis, G., Butiseacă, G.A., Antonarakou, A., Agiadi, K., Zarkogiannis, S.D., Krsnik, E., Besiou, E., Zachariasse, W.J., Lourens, L., Thivaiou, D., Koskeridou, E., 2022. Hypersalinity accompanies tectonic restriction in the eastern Mediterranean prior to the Messinian Salinity Crisis. Palaeogeography, Palaeoclimatology, Palaeoecology, 592, 110903.

Kremer, B., Kazmierczak, J., 2005. Cyanobacterial mats from Silurian Black radiolarian cherts: phototrophic life at the edge of darkness? Journal of Sedimentary Research, 75, 897–906.

Lazar, C.S., L'Haridon, S., Pignet, P., Toffin, L., 2011. Archaeal Populations in Hypersaline Sediments Underlying Orange Microbial Mats in the Napoli Mud Volcano. Applied and Environmental Microbiology, 77, 3120–3131.

Le Breton, E., Handy, M.R., Molli, G., Ustaszewski, K., 2017. Post-20 Ma motion of the Adriatic plate: New constraints from surrounding Orogens and implications for crust-mantle coupling. Tectonics, 36, 3135–3154.

Lesser, M. P., Slattery, M., Leichter, J.J., 2009. Ecology of mesophotic coral reefs. Journal Exploration in Marine Biology Ecology, 375, 1–8.

Levin, L.A., Baco, A.R., Bowden, D.A., Colaco, A., Cordes, E.E., Cunha, M.R., Demopoulos,

A.W.J., Gobin, J., Grupe, B.M., Le, J., Metaxas, A., Netburn, A.N., Rouse, G.W., Thurber, A.R., Tunnicliffe, V., Van Dover, C.L., Vanreusel, A., Watling, L., 2016. Hydrothermal Vents and Methane Seeps: Rethinking the Sphere of Influence. Frontiers in Marine Science 3, 1–23.

Lugli, S., Manzi, V., Roveri, M., Schreiber, B.C., 2010. The Primary Lower Gypsum in the Mediterranean: A new facies interpretation for the first stage of the Messinian salinity crisis. Palaeogeography, Palaeoclimatology, Palaeoecology, 297, 83–99.

Maignien, L., Parkes, R.J., Cragg, B., Niemann, H., Knittel, K., Coulon, S., Akhmetzhanov, A., Boon, N., 2013. Anaerobic oxidation of methane in hypersaline cold seep sediments: FEMS Microbiology Ecology, 83, 214–231.

Manzi, V., Lugli, S., Roveri, M., Schreiber, B.C., Gennari, R., 2011. The Messinian "Calcare di Base" (Sicily, Italy) revisited. Geological Society of America Bulletin, 123, 347–370.

Marini, M., Russo, A., Paschini, E., Grilli, F., Campanelli, A., 2006. Short-term physical and chemical variations in the bottom water of middle Adriatic depressions. Climate Research, 31, 227–237.

Mastandrea, A., Barca, D., Guido, A., Tosti, F., Russo, F., 2010. Carbonate deposition and diagenesis in evaporitic environments: The evaporative and sulphur-bearing limestones during the settlement of the Messinian Salinity Crisis in Sicily and Calabria. Carbonates and Evaporites, 25, 133–143.

Meyers, P.A., 1994. Preservation of elemental and isotopic source identification of sedimentary organic matter. Chemical Geology, 114, 289–302.

Milkov, A.V., Etiope, G., 2018. Revised genetic diagrams for natural gases based on a global dataset of >20,000 samples. Organic Geochemistry, 125, 109–120.

Montanari, D., Del Ventisette, C., Bonini, M., Sani, F., 2007. Passive-roof thrusting in the

Messinian Vena del Gesso Basin (Northern Apennines, Italy): constraints from field data and analogue models. Geological Journal, 42, 455–476.

Natalicchio, M., Dela Pierre, F., Clari, P., Birgel, D., Cavagna, S., Martire, L., Peckmann, J., 2013. Hydrocarbon seepage during the Messinian salinity crisis in the Tertiary. Piedmont Basin (NW Italy). Palaeogeography, Palaeoclimatology, Palaeoecology, 390, 68–80.

Oliveri, E., Neri, R., Bellanca, A., Riding, R., 2010. Carbonate stromatolites from a Messinian hypersaline setting in the Caltanissetta Basin, Sicily: Petrographic evidence of microbial activity and related stable isotope and rare earth element signatures. Sedimentology, 57, 142–161.

Orcutt, B.N., Joye, S.B., Kleindienst, S., Knittel, K., Ramette, A., Reitz, A., Samarkin, V., Treude, T., Boetius, A., 2010. Impact of natural oil and higher hydrocarbons on microbial diversity, distribution, and activity in Gulf of Mexico cold-seep sediments. Deep-Sea Research Part II: Topical Studies in Oceanography, 57, 2008–2021.

Oren, A., 2011. Thermodynamics limits to microbial life at high salt concentrations. Environmental Microbiology, 13, 1908–1923.

Paul, H.A., Bernasconi, S.M., Schmid, D.W., McKenzie, J.A., 2001. Oxygen isotopic composition of the Mediterranean Sea since the Last Glacial Maximum: constraints from pore water analyses. Earth and Planetary Science Letters, 192, 1–14.

Peckmann, J., Thiel, V., Reitner, J., Taviani, M., Aharon, P., Michaelis, W., 2004. A Microbial Mat of a Large Sulfur Bacterium Preserved in a Miocene Methane-Seep Limestone. Geomicrobiology Journal, 21, 247–255.

Peryt, T. M., 1981. Phanerozoic oncoids — an overview. Facies, 4, 197–214.

Perri, E., Gindre-Chanu, L., Caruso, A., Cefal, M., Scopelliti, G., Tucker, M., 2017. Microbial-mediated pre-salt carbonate deposition during the Messinian salinity crisis (Calcare di Base Fm.,

Southern Italy). Marine and Petroleum Geology, 88, 235–250.

Rigaudier, T., Lécuyer, C., Gardien, V., Suc, J.P., Martineau, F., 2011. The record of temperature, wind velocity and air humidity in the δD and $\delta^{18}O$ of water inclusions in synthetic and Messinian halites. Geochimica et Cosmochimica Acta, 75, 4637–4652.

Rouchy, J.M., Monty, C. (2000). Gypsum Microbial Sediments: Neogene and Modern Examples. In: Riding, R.E., Awramik, S.M. (eds) Microbial Sediments. Springer, Berlin, Heidelberg. https://doi.org/10.1007/978-3-662-04036-2_23

Rouchy, J.M., Caruso, A., 2006. Review. The Messinian salinity crisis in the Mediterranean basin: A reassessment of the data and an integrated scenario. Sedimentary Geology, 188–189, 35–67.

Sahling, H., Rickert, D., Lee, R.W., Linke, P., Suess, E., 2002. Macrofaunal community structure and sulfide flux at gas hydrate deposits from the Cascadia convergent margin, NE Pacific. Marine Ecology Progress Series, doi:10.3354/meps231121.

Schulz, H.N., Brinkhoff, T., Ferdelman, T.G., Mariné, M.H., Teske, A., Jørgensen, B.B., 1999. Dense Populations of a Giant Sulfur Bacterium in Namibian Shelf Sediments. Science 284, 493–495.

Smrzka, D., Zwicker, J., Klügel, A., Monien, P., Bach, W., Bohrmann, G., Peckmann, J., 2016. Establishing criteria to distinguish oil-seep from methane-seep carbonates. Geology, 44, 667–670.

Stranne, C., O'Regan, M., Hong, Wei-Li., Brüchert, V., Ketzer, M., Thornton, B., Jakobsson, M., 2022. Anaerobic oxidation has a minor effect on mitigating seafloor methane emissions from gas hydrate dissociation. Communications Earth and Environment, 3, 163. https://doi.org/10.1038/s43247-022-00490-x .

Suess, E., 2014. Marine cold seeps and their manifestations: geological control, biogeochemical

criteria and environmental conditions. International Journal of Earth Sciences, 103, 1889–1916.

Terzi, C., Ricci Lucchi, F.R., Vai, G.B., Aharon, P., 1994. Petrography and stable isotope aspects of cold-vent activity imprinted on Miocene-age "calcari a *Lucina*" from Tuscan and Romagna Apennines, Italy. Geo-Marine Letters, 14, 177–184.

Torres, M.E., Brumsack, H.J., Bohrmann, G., Emeis, K.C., 1996. Barite fronts in continental margin sediments: A new look at barium remobilization in the zone of sulfate reduction and formation of heavy barites in diagenetic fronts. Chemical Geology, 127, 125–139.

Tzevahirtzian, A., Caruso, A., Scopelliti, G., Baudin, F., Blanc-Valleron, M.M., 2022. Onset of the Messinian Salinity Crisis: Sedimentological, petrographic and geochemical characterization of the pre-salt sediments from a new core (Caltanissetta Basin, Sicily). Marine and Petroleum Geology, 141, 105686.

Vai, G.B., Ricci Lucchi, F., 1977. Algal crusts, autochthonous and clastic gypsum in a cannibalistic evaporitic basin: a case history from the Messinian of the Northern Apennines. Sedimentology, 24, 211–244.

Vasconcelos, C., McKenzie, J., Warthmann, R., Bernasconi, S., 2005. Calibration of the $\delta^{18}O$ paleothermometer for dolomite precipitated in microbial cultures and natural environments. Geology, 33, 317–320.

Ziegenbalg, S.B., Brunner, B., Rouchy, J.M., Birgel, D., Pierre, C., Böttcher, M.E., Caruso, A., Peckmann, J., 2010. Formation of secondary carbonates and native sulphur in sulphate-rich Messinian strata, Sicily. Sedimentary Geology, 227, 37–50

Ziegenbalg, S.B., Birgel, D., Hoffmann-Sell, L., Pierre, C., Rouchy, J.M., Peckmann, J., 2012. Anaerobic oxidation of methane in hypersaline Messinian environments revealed by ^{13}C-depleted molecular fossils. Chemical Geology, 292–293, 140–148.

CAPTIONS

Fig. 1. A) Schematic geological map of the northern Apennines showing the distribution of the Miocene Marnoso-arenacea Fm and of Messinian evaporites (Gessoso-Solfifera Fm) represented by the red line. The location of the investigated area is indicated (star). B) Location of the studied outcrops: Co di Sasso= 44°14'17.81" N; 11°42'36.43"E; M. Spugna= 44°13'32.96" N;11°43'35.97"E; Abisso Mornig= 44°13'58.58" N; 11°44'05.58"E; Parco Carnè= 44°13'42.49" N; 11°44'13.37"E; Abisso Carnè= 44°13'26.43" N; 11°44'22.12"E; Rontana= 44°13'18.59" N; 11°44'26.26"E; Case Torre= 44°14'08.29" N; 11°44'06.96"E.

Fig. 2. Stratigraphic logs of the studied seep carbonate outcrops showing vertical sedimentary facies changes from the euxinic shales to the Messinian evaporites. Precise location in Fig 1. The vertical scale is in meters.

Fig. 3. Carbonate facies in the examined outcrops: A) Concordant passage from the massive carbonates (left) to the laminated and stromatolitic carbonates in the Cò di Sasso outcrop (the bedding is sub-vertical); B) Laminated facies up section in Mt Spugna outcrop; C) Concordant passage (dotted line) of laminated carbonates to gypsum in the Cò di Sasso outcrop; the bedding attitude is sub-vertical; D) Passage from seep carbonates with large bivalves in the lower part to laminated facies (Abisso Mornig outcrop); E) Large lucinid in the massive facies (Mt. Spugna).

Fig. 4. Photomicrographs of the massive facies. PPL: plane polarized light; XPL: cross-polarized light; CL: cathodoluminescence image; BSE: back-scattered electron image. A) PPL image of the micritic-microsparitic sediment composing the massive facies. Sample AC-10 from Casa Torre. B) PPL image of the spheroidal dolomite (Dol) filling a cavity in the massive facies, followed by calcite spar (Cal). Sample AC-10 from Casa Torre. C) Massive facies dominated by early-

diagenetic dolomicrite (Dol; dark grey) with abundant calcitic (Cal; light grey) allochems, predominantly planktonic foraminiferal tests, some of which filled by late intragranular calcite cement. Sample AC-2 from Grotta Carnè (BSE image). D) CL image of B: note the zonation of the dolomite spheroids.E-F) PPL image of micritic filaments (black arrows) preserved within peloidal deposits. Sample AC-10 from Casa Torre.

Fig. 5. Photomicrographs of the transitional facies. PPL: plane polarized light; XPL: cross-polarized light; BSE: back-scattered electron image. A) PPL image of the microcrystalline clotted micrite composing the transitional facies. Sample AC-11 from Casa Torre. B) Transitional facies with authigenic dolomite (Dol; dark grey), acicular aragonite (Ar, light grey), and authigenic intergranular and cavity-filling barite (Brt; white); detrital quartz (Qtz; very dark grey) is present, Sample AC-11 from Casa Torre (BSE image). C-D) Transitional facies comprising micro oncoid-like grains composed of dolomite which are overgrown by acicular aragonite, followed by drusy dolomite and calcite cements. Note also detrital biotite (Bt). Sample AC-11 from Casa Torre (BSE image). E) Traces of washout surface (dashed white line) in peloidal carbonates interpreted as microbial deposits; below the surface peloidal packstones with traces of oxidized pyrite grains (dark); above the surface peloidal grainstones with sparitic envelops and large pore spaces, both filled with sparite (white) or empty (dark). Sample AC-11 from Casa Torre (PPL image). F) Large oncoid-like grain showing concentric sparitic-micritic envelopes, surrounded by smaller peloids and aggregates of peloids; note tiny oxidized pyrite grains and pores lined with drusy calcite cements. Sample AC-11 from Casa Torre (PPL image).

Fig. 6. Photomicrographs of the laminated facies. PPL: plane polarized light; XPL: cross-polarized light; BSE: back-scattered electron image. A) Dark dolomicrite laminae alternated with light microscrystalline calcite. Sample GB2 from Abisso Mornig PPL images. B) Peloidal particles made of dolomicrite within a microspatitic cement: Sample CDS2 from Cò di Sasso.

PPL image. C) peloidal-clotted dolomicrite forming thin dark laminae and elongated curved aggregates in a microsparitic groundmass: Sample GB18 from Monte Spugna, PPL image. D) BSE image of the zoned dolomite. Note the concentrical growth. E) Poikilotopic celestine crystals (Cel; white) in the microcrystalline calcitic groundmass of the laminated facies from Co' di Sasso (sample CDS-3). BSE image. F) Densely packed oncoid-like grains of various sizes, some of them forming aggregates, showing grading; coarse-crystalline calcite vein cuts the lower part of the sample, note dark traces of oxidized pyrite grains and aggregates of grains. Sample AC-12 from Casa Torre (PPL image).

Fig. 7. SEM images of HCl etched samples of carbonate deposits showing features typical of microbialites: (A-B) details of wavy lamination with laminae containing microbial structures, (C-F) characteristic pits and walls forming pattern interpreted as product of early diagenetic mineralization (calcitization?) of coccoid cyanobacterial mats (see explanations in the text), (G), remnants of organic sheaths binding carbonate grains (arrows) in laminated deposits, (H-I) peloids and micritic grains with concentric structure in micrite matrix, (J-K) modern mineralized with calcium carbonate cyanobacterial mat from Sulejów Dam, Poland (J), and subfossil coccoid cyanobacterial mat from the Satonda crater lake, Indonesia (K), mineralized with calcium carbonate, both showing similar appearance to web-like structures in studied samples illustrated in C-F. A-G (samples AC12), H, I (samples AC11). K, Photo courtesy of J. Kaźmierczak.

Fig. 8 Isotopic composition ($\delta^{13}C$, $\delta^{18}O$) of carbonate samples from different microfacies (see Table 1).

Fig. 9. Box and whisker plot for the calculated $\delta^{18}O$ of the parent bottom water at 11°C (see the text for details) for the three facies distinguished.

Table 1. Carbonate mineralogy, $\delta^{13}C$ and $\delta^{18}O$ values, and calculated $\delta^{18}O$ of the parent bottom water at 11°C (see the text for details) for samples from Cò di Sasso, Casa Torre, Abisso Mornig, and Grotta Carné representing all three facies. The relative content of foraminifera is also reported. Carbonate mineralogy was established by thin section petrography, SEM and quantitative XRD analysis.

Section	Sample	Facies	Relative content of carbonate minerals*	Relative content of foraminifera**	$\delta^{18}O_{carb}$ (‰)	$\delta^{13}C_{carb}$ (‰)	$\delta^{18}O$ (‰) of bottom water at 11ºC
Cò di Sasso	CDS3a	laminated	Cal 100%	-	-6.5	-12.2	-7.7
	CDS3b	laminated	Cal 100%	-	-6.1	-12.4	-7.4
	CDS2a	laminated	Cal 100%	-	-7.3	-6.9	-8.5
	CDS2b	laminated	Cal 100%	-	-7.4	-6.3	-8.7
	CDS1a	laminated	Cal 100%	-	-6.8	-11.6	-8.1
	CDS1b	laminated	Cal 100%	-	-7.2	-7.7	-8.5
	CDS1m	massive	no data	no data	0.1	-22.4	not calculated
Casa Torre	GB-3a	laminated	Dol 80%, Cal 20%	-	4.2	-39.9	0.8
	GB-3b	laminated	Dol 80%, Cal 20%	-	4.8	-38.3	1.5
	GB-3c	laminated	Dol 80%, Cal 20%	-	4.3	-36.2	1.0
	AC-12	laminated	Dol 90%, Cal 10%	-	5.2	-44.6	1.6
	AC-11	transitional	*Ar 60%, Dol 23%, Cal 17%*	+	3.3	-14.4	1.4
	AC-10	transitional	*Cal 69%, Dol 22%, Ar 9%*	+	4.1	-35.3	2.3
	AC-9	massive	*Cal 100%*	++	-2.5	-34.2	-3.8
	AC-8	massive	*Cal 86%, Dol 14%*	no data	0.1	-47.5	-1.6
	AC-7	massive	*Dol 51%, Cal 36%, Ar 13%*	no data	2.0	-45.0	-0.6
Abisso Mornig	GB-2	laminated	Dol 90%, Cal 10%	-	4.8	-28.0	1.2
	36-B	transitional	*Cal 100%*	no data	-2.7	-38.5	-4.0
	36-Cb	transitional	Cal 100%	++	0.8	-43.8	-0.5
	36-Ca	massive	Cal 100%	+++	-4.2	-25.2	-5.5
	36-A	massive	*Cal 100%*	no data	-5.3	-36.1	-6.6
	GB-1a	massive	Dol 90%, Cal 10%	++	0.3	-49.1	-3.3
	GB-1b	massive	Dol 90%, Cal 10%	++	-0.3	-39.9	-3.9
Grotta Carnè	AC-6c	laminated	Dol 98%, Cal 2%	-	4.1	-51.2	0.3
	AC-6b	transitional	Dol 95%, Cal 5%	+	2.6	-48.5	-1.1
	AC-6a	transitional	Dol 98%, Cal 2%	-	4.1	-47.7	0.3
	AC-4	massive	*Dol 77%, Cal 14%, Ar 9%*	++	1.7	-42.3	-1.5
	AC-3b	massive	Dol 80%, Cal 15%, Ar 5%	+++	2.8	-47.4	-0.6
	AC-3c	massive	Dol 80%, Cal 15%, Ar 5%	+++	3.0	-39.2	-0.3
	AC-2	massive	Dol 80%, Cal 15%, Ar 5%	+++	3.3	-40.4	-0.1

*Estimated on the basis of petrographic investigations (normal font) or quantitative XRD analysis (italics)

**The number of "+" indicates the relative abundance of calcitic foraminiferal tests; "-" indicates absence of foraminifera

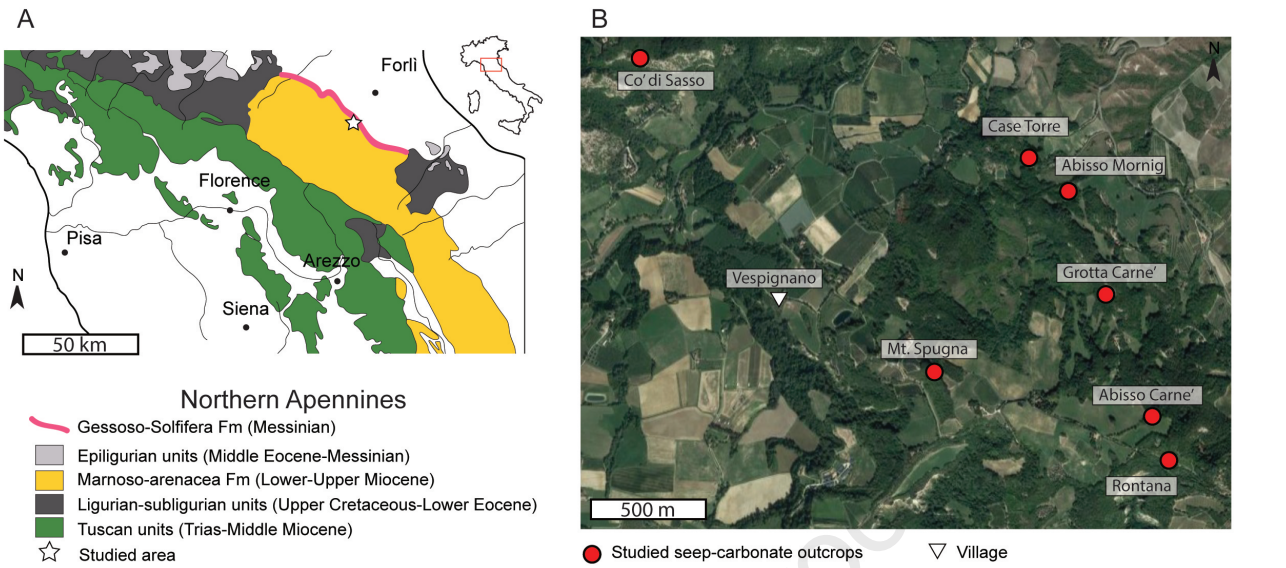

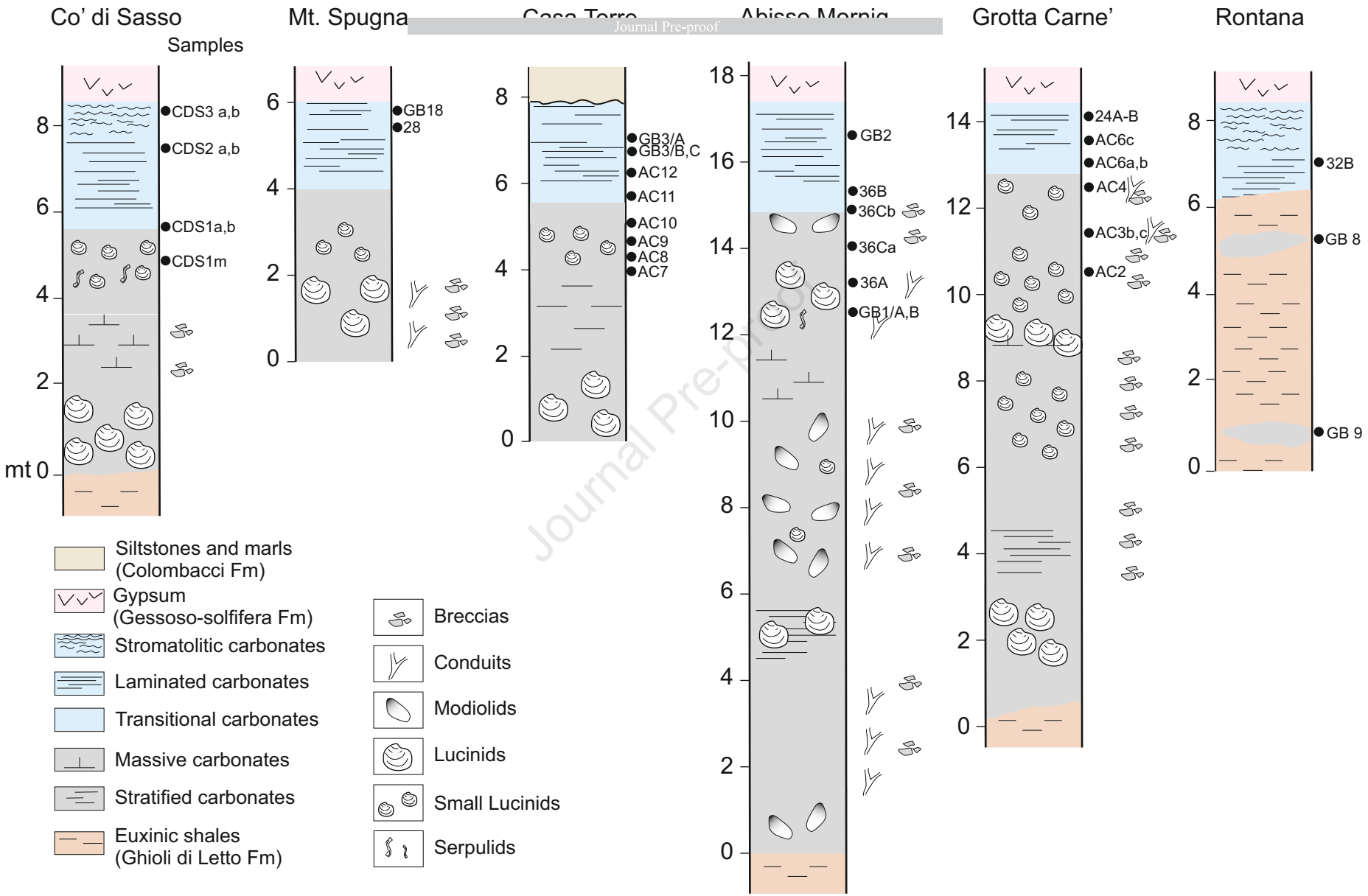

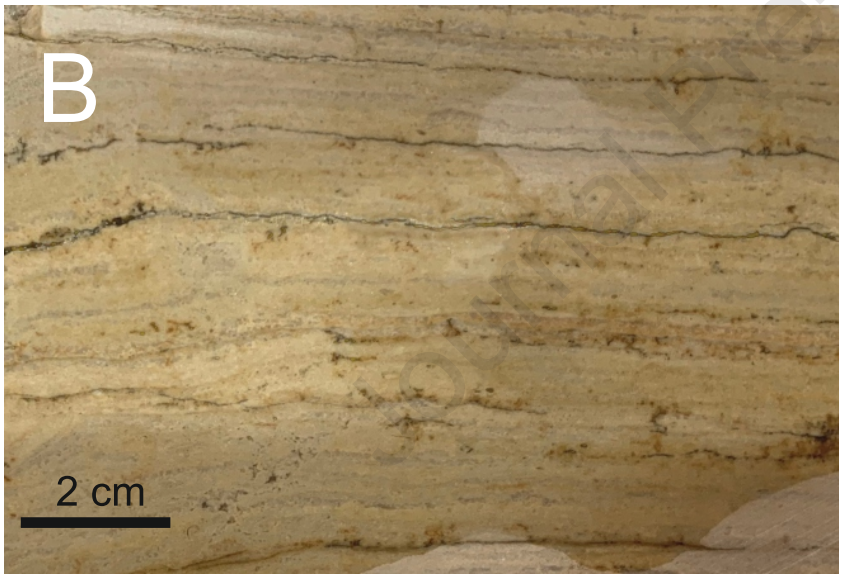

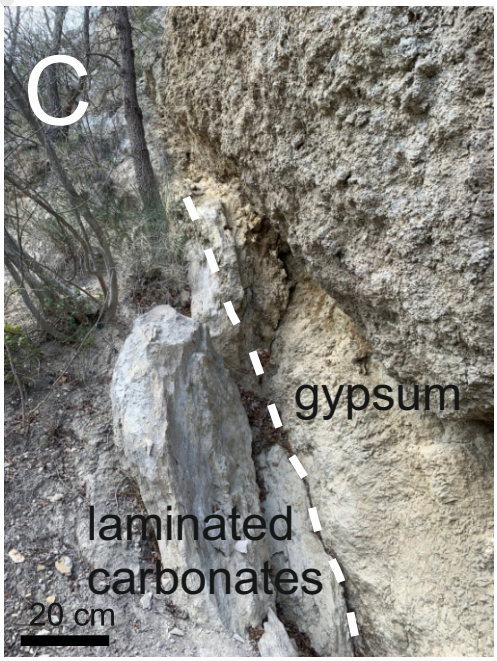

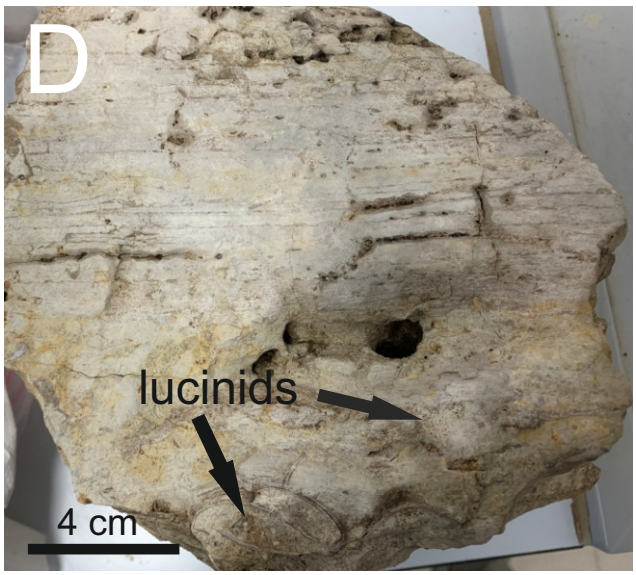

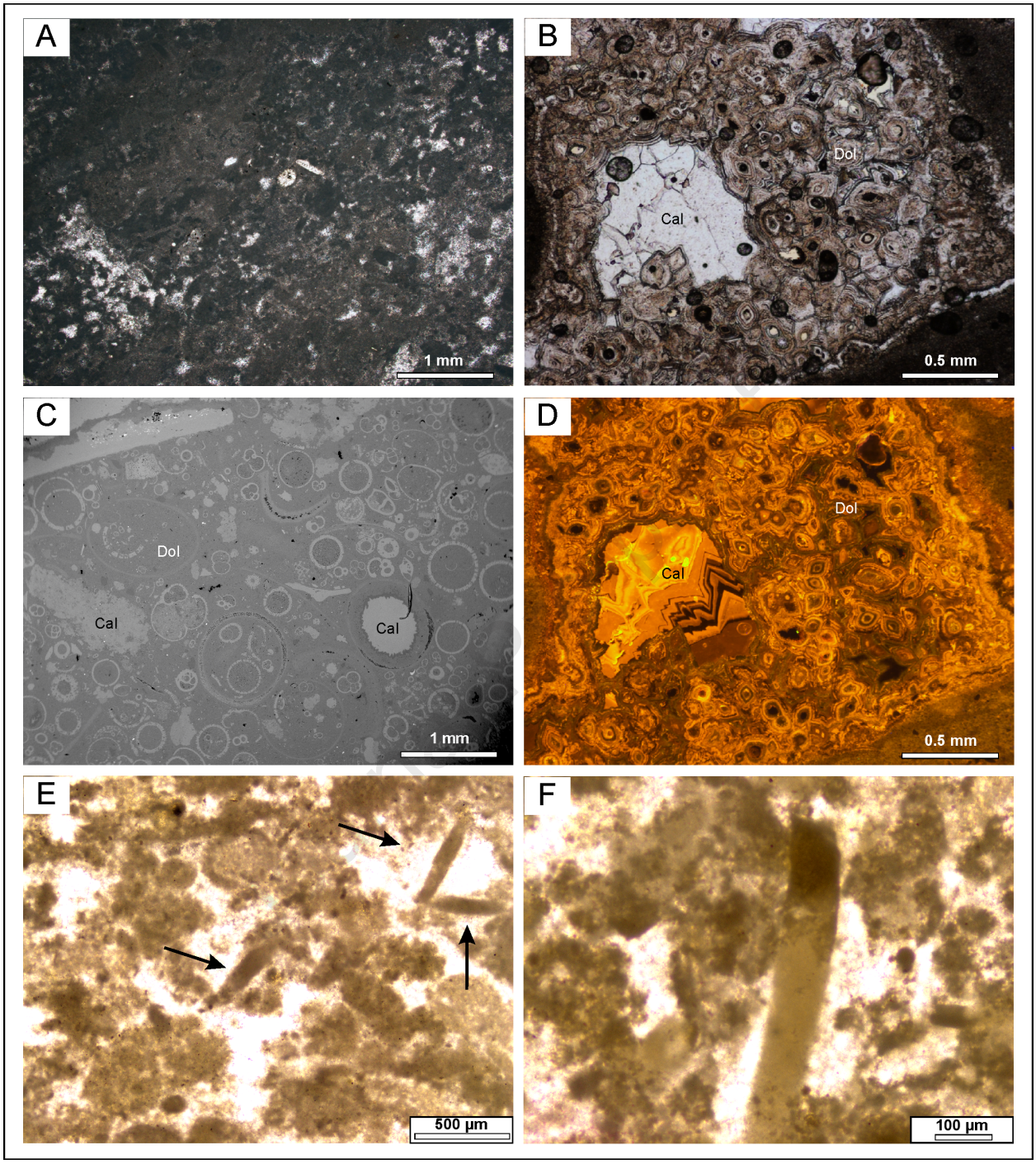
A
1 mm
B
Dol
Cal
0.5 mm
C
Dol
Cal
Cal
1 mm
D
Dol
Cal
0.5 mm
E
500 µm
F
100 µm

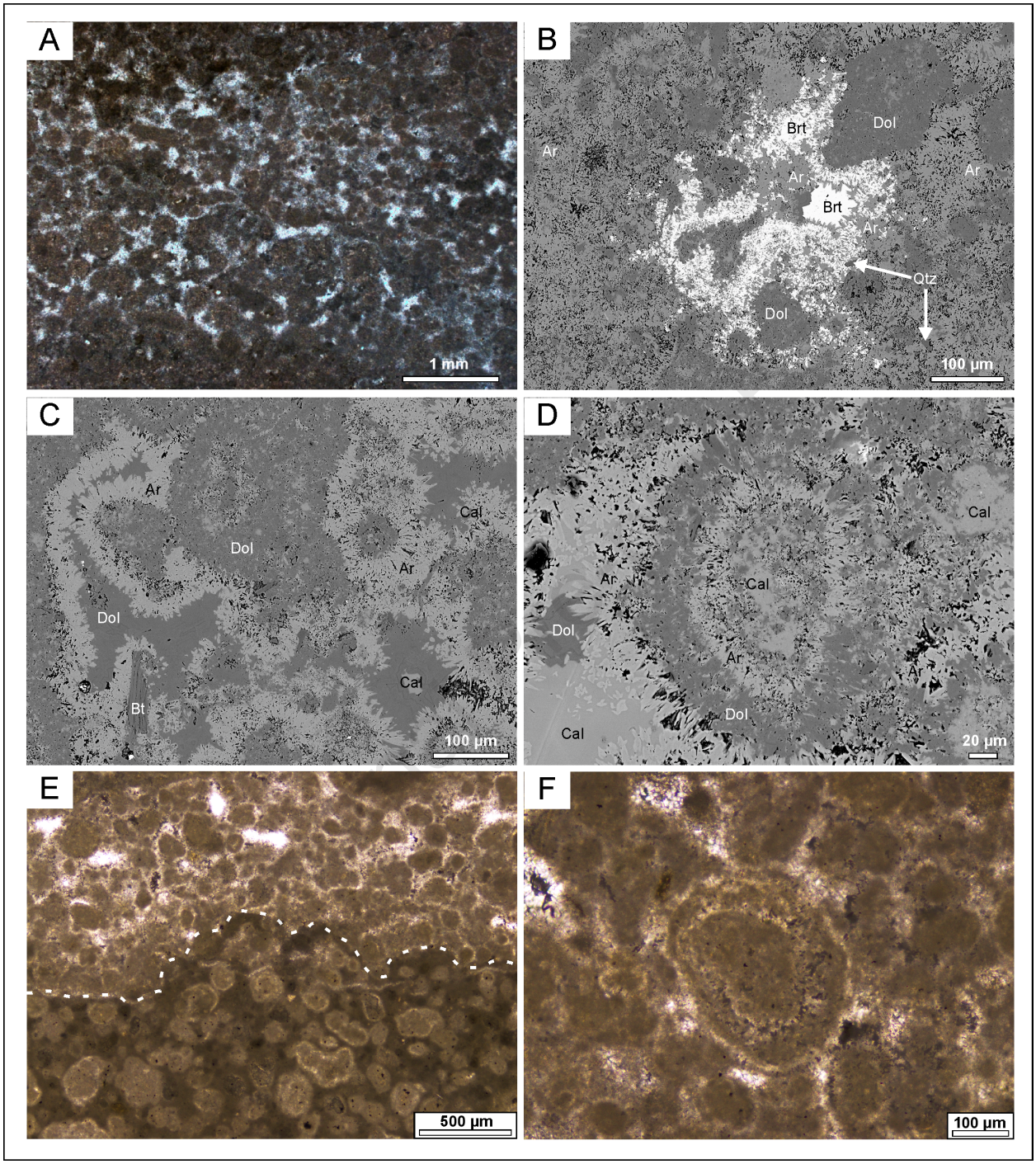
A
1 mm
B
Brt
Dol
Ar
Ar
Ar
Brt
Ar
Qtz
Dol
100 µm
C
Ar
Cal
Dol
Ar
Dol
Cal
Bt
100 µm
D
Cal
Ar
Cal
Dol
Ar
Ar
Dol
Cal
20 µm
E
500 µm
F
100 µm

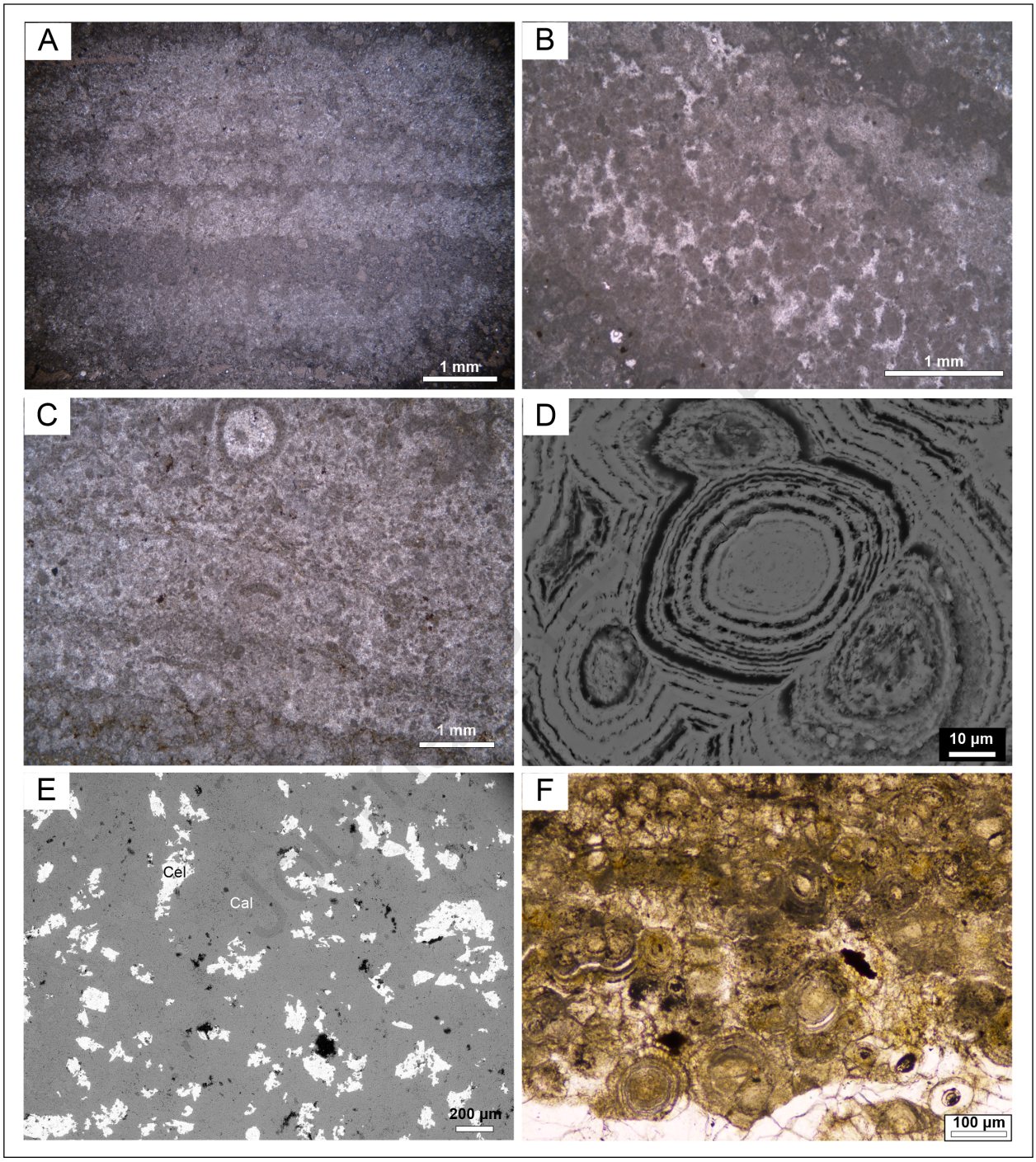
A
1 mm
B
1 mm
C
1 mm
D
10 µm
E
Cel
Cal
200 µm
F
100 µm

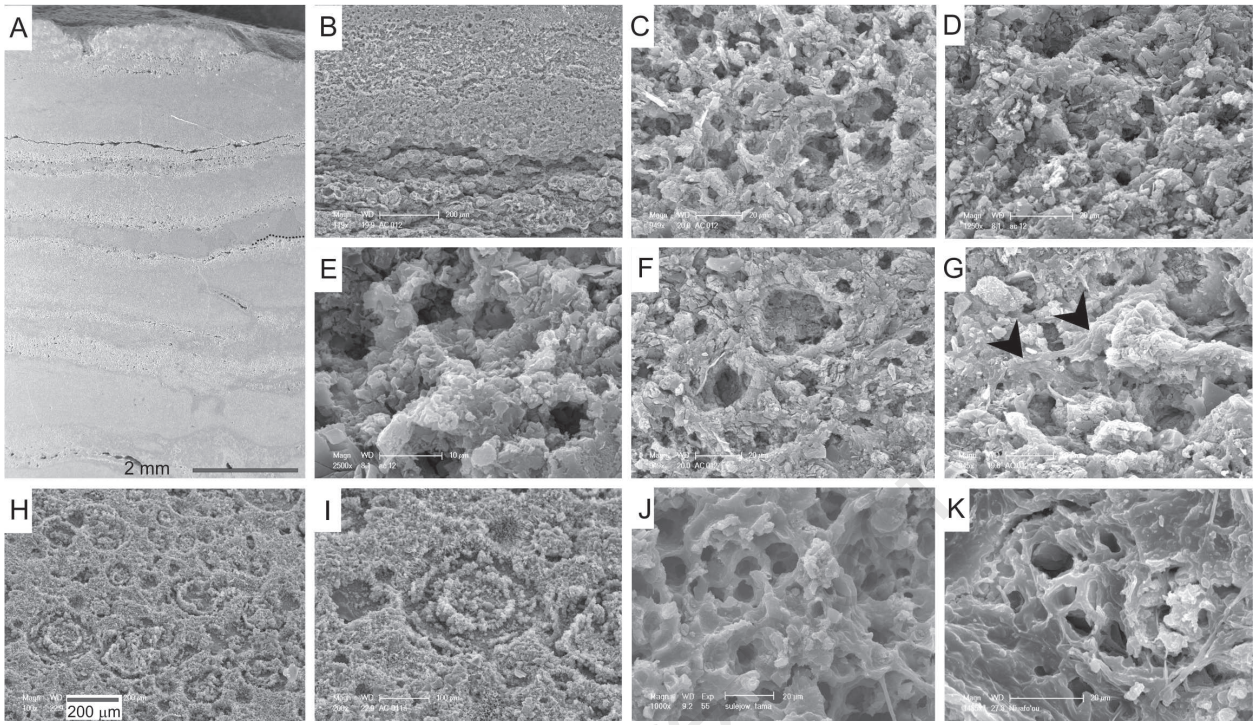

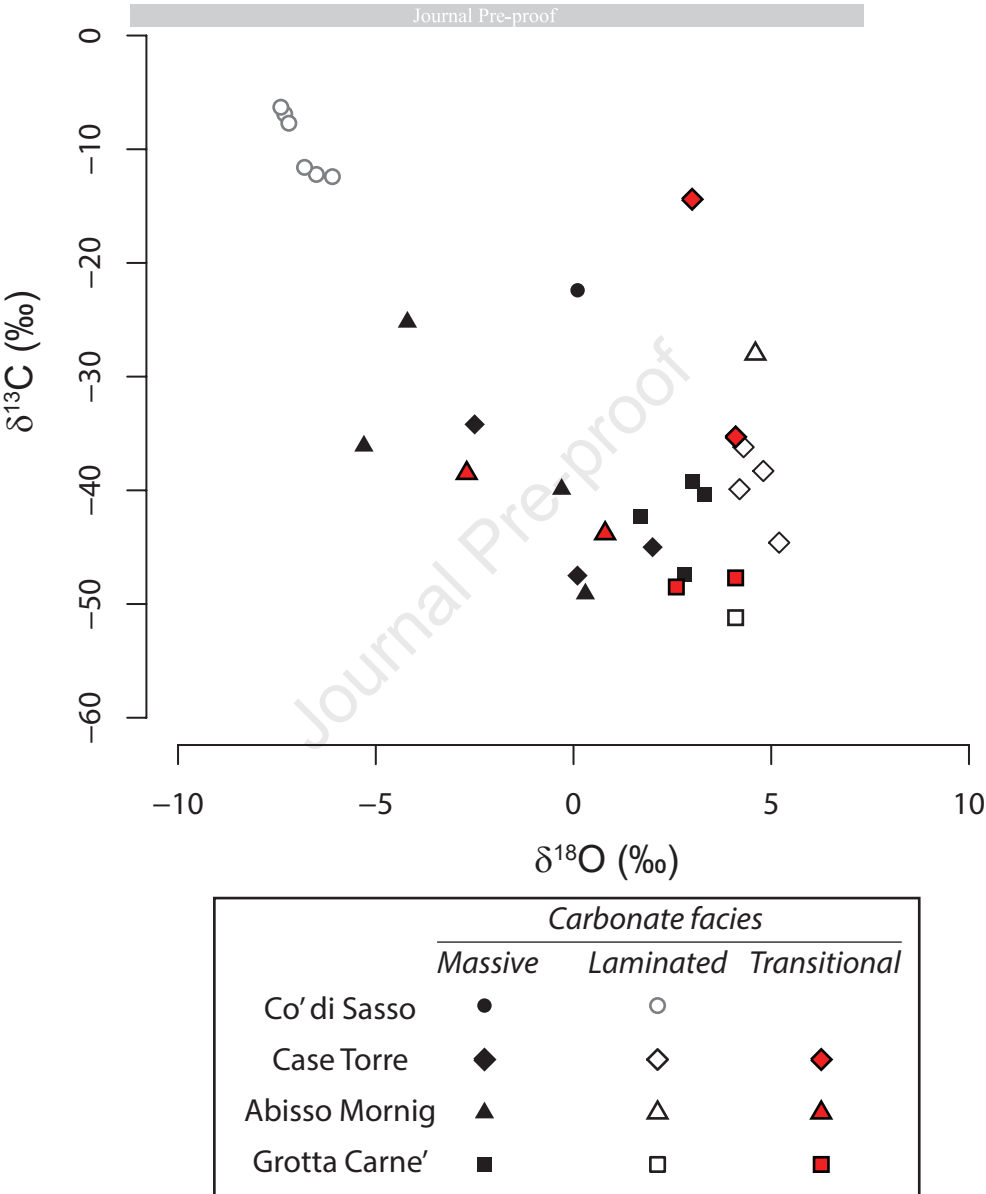

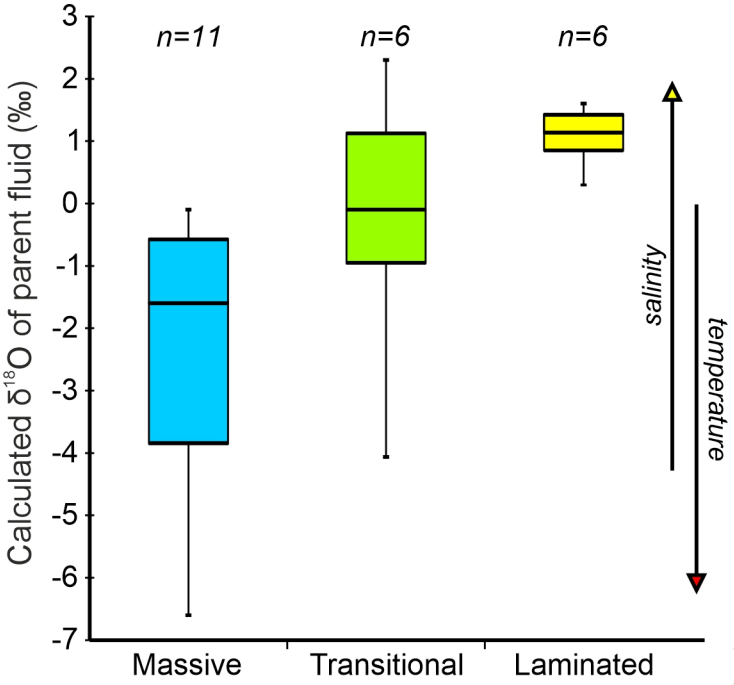

Seep carbonates preceding the Messinian evaporites in the northern Apennines record the transition from marine to higher stressed evaporitic conditions

The transition from massive seep carbonates to laminated carbonates is associated with abrupt loss of macrofauna and predominance of dolomite over calcite.

Microbial fabrics preserved in the Messinian seep-carbonates indicate that cyanobacterial communities played a significant role in the formation of carbonate deposits

The δ18O rise from the massive, through transitional, to the laminated facies reflects either a drop of bottom water temperature or a rise of salinity.

Declaration of interests

☒ The authors declare that they have no known competing financial interests or personal relationships that could have appeared to influence the work reported in this paper.

☐ The authors declare the following financial interests/personal relationships which may be considered as potential competing interests: